Model oxide supported MoS2 HDS catalysts: structure and surface properties

"Model oxide supported MoS2 HDS catalysts: Structure and surface properties"

Catalysis Science and Technology
Volume 1, Issue 1, April 2011, Pages 123-136
DOI: 10.1039/c0cy00050g

By Federico Cesano, Serena Bertarione, Andrea Piovano, Giovanni Agostini, Mohammed Mastabur Rahman, Elena Groppo, Francesca Bonino, Domenica Scarano, Carlo Lamberti, Silvia Bordiga, Luciano Montanari, Lucia Bonoldi, Roberto Millini and Adriano Zecchina

Model oxide supported MoS_2 HDS catalysts: structure and surface properties

Federico Cesano[a],Serena Bertarione[a], Andrea Piovano[a], Giovanni Agostini[a], Mohammed Mastabur Rahman[a], Elena Groppo[a], Francesca Bonino[a], Domenica Scarano[a], Carlo Lamberti[a], Silvia Bordiga[a], Luciano Montanari[b], Lucia Bonoldi[b], Roberto Millini[b] and Adriano Zecchina[*a]

[a]*Department of Inorganic, Physical and Materials Chemistry, NIS Centre of Excellence, and Centre of Reference INSTM, University of Turin, Via P. Giuria 7, I-10125, Torino, Italy*

[b] *Eni S.p.A., Refining & Marketing Division, Research and Technological Development, Research Center, Via Maritano 26, I-20097 San Donato Milanese (MI), Italy*

Cover

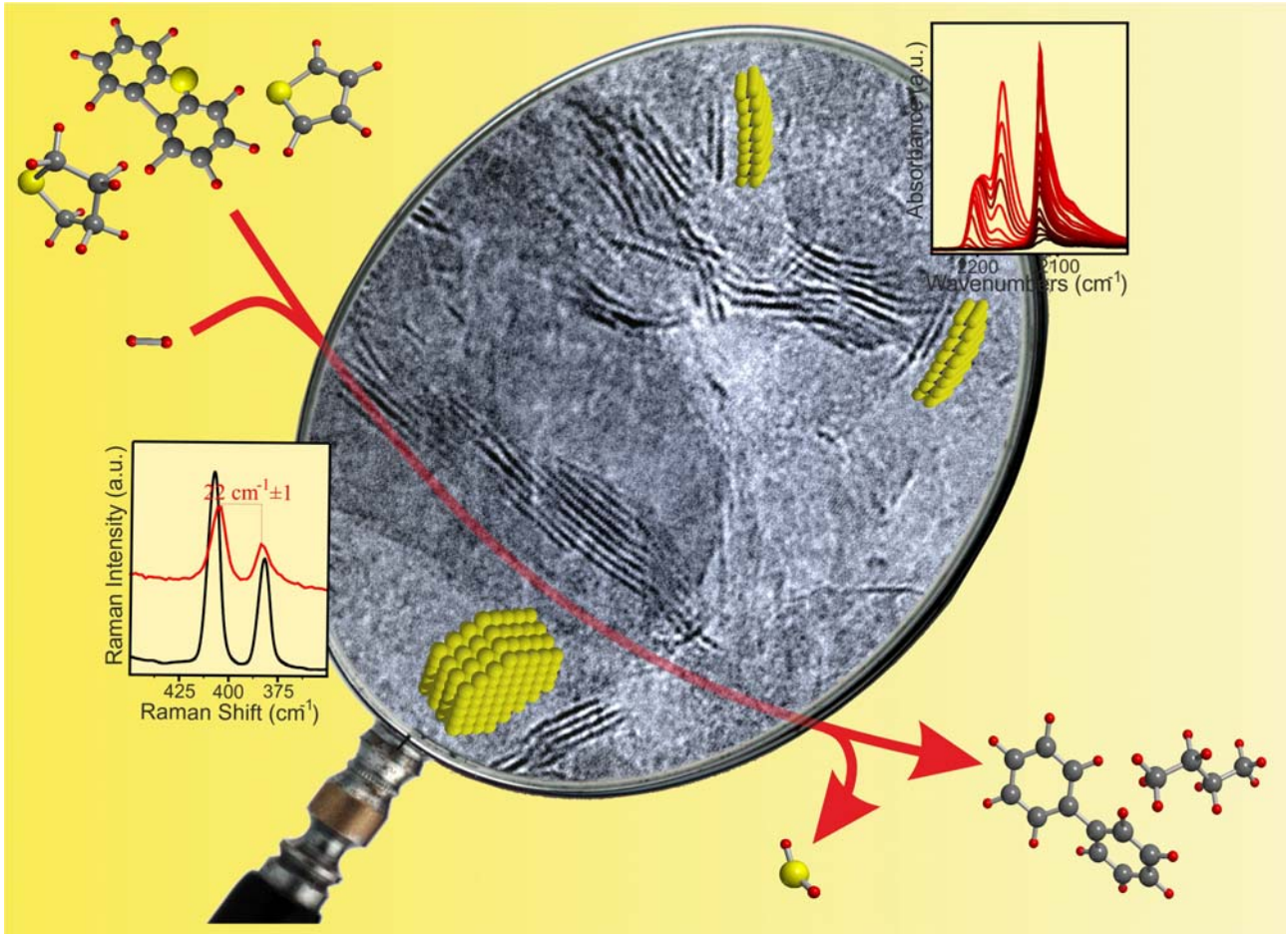

* Corresponding author. e-mail: adriano.zecchina@unito.it. Fax: +39 011 6707855 Tel: +39 011 6707860

Abstract

Supported hydrodesulfidation (HDS) MoS_2/SiO_2, MoS_2/γ-Al_2O_3 and MoS_2/MgO catalysts having a model character have been synthesized starting from the corresponding supported Mo oxide by using CS_2 as sulfiding agent and deeply investigated by means of several techniques.
XRPD, HRTEM, Raman and UV-Vis characterization methods have been applied to obtain information on the morphology and the structure of the catalysts (including degree of staking and structural disorder) as well as on the vibrational and spectroscopic properties. It is shown that, when compared with HRTEM results, XRPD, Raman and UV-Vis data give a realistic information on the staking degree, on the particle size distribution and on the heterogeneity of supported MoS_2 particles on the various supports. EXAFS and XANES spectroscopies have been also used to set up the best sulfidation procedure on the MoS_2/SiO_2 system, and the obtained recipe has been adopted for the MoS_2/γ-Al_2O_3 and MoS_2/MgO systems. UV-vis analysis under controlled atmosphere has been performed to understand the effect of reductive and sulfiding treatments on the presence of sulfur vacancies and on the valence state of Mo ions associated with them. To explore the structure of coordinatively unsaturated Mo sites after reducing or sulfiding treatments (with CS_2 or, occasionally, with H_2S), in situ FTIR of CO adsorbed at low-temperature has been performed on all samples. It is demonstrated that CO is a sensitive probe for coordinatively unsaturated sites and that the formation of sulfur vacancies on the MoS_2 surface upon reduction in pure H_2 at 673 K is accompanied by an increase of the coordinative unsaturation and a decrease of the valence state of a fraction of surface Mo cations, mainly located on corner and edge sites. Considering the non planarity of a consistent fraction of lammelae (as revealed in particular by HRTEM of MoS_2 on Al_2O_3 and MgO), the presence of reducible Mo ions, located in defective positions on basal planes, cannot be excluded. Furthermore, it is demonstrated that this process can be reversed upon interaction with the sulfiding agent and that this reversible behavior is really mimicking some of the elementary acts occurring in the HDS process. Comparing the results obtained by all the adopted characterization techniques, it is concluded that the reductive effect of H_2 preferentially affects the particles characterized by the lowest staking degree. The complexity of the IR results suggests that the adopted reduction procedure in pure H_2 at 673 K induces the formation of several type of sulfur vacancies, presumably located in different crystallographic positions of the MoS_2 particles. In conclusion, the IR results obtained with the CO probe fully support the idea that the adopted reduction procedure in pure H_2 at 673 K is not only inducing the formation of several families of sulfur vacancies but that a continuity exists between the stages associated with the reduction of the different sites, those located on the planar base being the latest to be reduced. It is also concluded, that the sulfiding steps are strongly involving the surface of the support and that reductive treatments at high T in H_2 are causing sulfur depletion not only from supported MoS_2 particles, but also from the supporting phase. The involvement of the support is particularly relevant for supports (Al_2O_3 and MgO) which are characterized by: i) extensive $O^{=}/S^{=}$ surface exchange reactions during the sulfidation steps ; ii) strong MoS_2/support interaction and iii) increasing dispersion. It is concluded that the properties described in i-iii) are interconnected.

Keywords: Molybdenum sulfide (MoS_2), Hydrodesulfidation, TEM, XRPD, EXAFS, XANES, Raman, FTIR, UV-Vis-NIR

1. Introduction

Molybdenum sulfide compounds find many applications in several fields, such as chemical sensors,[1] solar cells,[2] low-friction surface applications[3] and in catalysis.[4-7] In particular, MoS_2 is a widely used catalyst in hydrotreatment processes, like hydrodesulfidation (HDS) and CO hydrogenation, for the production of cleaner fuels in the oil refining industry. Hydrotreatment catalysts are probably the best described among heterogeneous catalysts, because there is a large amount of experimental and theoretical research devoted to these strategic materials.[8-10]
It is usually accepted that the active phase of HDS catalysts is constituted by small nanoparticles (average diameter 5 nm) of lamellar MoS_2, in form of sandwiched S-Mo-S layers (slabs), stacked on top of each other and separated by van der Waal's gaps. It has been shown that in many alumina-supported systems, the MoS_2 phase is highly dispersed and single slab structures might dominate.[11, 12]

Unsupported MoS_2 nanoparticles constituted by a single layer were studied by atomically resolved scanning tunneling microscopy (STM), in order to achieve atomic-scale insight into the mechanism of interaction with hydrogen and sulfur-containing molecules (such as thiophene).[13, 14] It was shown that, depending on the synthesis and sulfidation conditions, MoS_2 nanoparticles adopt triangular or hexagonally truncated morphologies. The MoS_2 triangular slabs are terminated by dimer-saturated Mo edges, while the hexagonal MoS_2 structures exhibit both Mo-edge and S-edges terminations. Furthermore, STM measurements showed that thiophene molecules adsorb and react on the fully sulfided edges of triangular single-layer MoS_2 nanoplatelets, where special brim sites with a metallic character exist. As a consequence, the activity in HDS reactions has been attributed to sites located at particle edges and has been thought to be originated from sulfur vacancies or so-called coordinatively unsatured sites (*cus* sites),[9, 15-17] which are created by stripping off one or more sulfur atoms from the MoS_2 nanoparticles edges, during the treatment in hydrogen. The behavior of MoS_2 platelets towards hydrogen has been studied by means of TPR technique [16, 18] and several sulfur species have been distinguished. The most weakly bonded species were assigned to the so called "extra sulfur" in MoS_{2+x} samples, *i.e.* samples sulfided in absence of hydrogen. The depletion of these species originates a TPR peak at about 520K.[16] The "stoichiometric" sulfur reacts with H_2 forming H_2S and sulfur vacancies in the 473-873 K range only [16, 18] and it is ascertained that small particles are much more reducible than the larger ones. No definite conclusion has been advanced on the relative propensity of sulfur anions located on defects, corners, edges and on extended faces to undergo depletion upon hydrogen treatment, although there is a complete agreement that sulfur ions located on extended faces will be the last to be depleted. In this regard, spectroscopic data have indicated that S-H species are present at the MoS_2 edges,[17, 19] and it was proposed that S-H groups may play a key role in supplying the hydrogen during HDS reaction. The matter of sulfur coverage level on edge sites has been discussed by several other authors[8, 10, 20-22] and the overall conclusion that can be drawn is that the sulfur coverage on the edges decreases with increasing reduction conditions (high hydrogen pressure and temperature).
Notwithstanding the large amount of literature on the topic, up to now the exact nature of the active sites for HDS on MoS_2 platelets dispersed on metal oxide supports and characterized by a low degree of structural definition is still not fully characterized. It is a matter of fact that the overall trends in catalytic activities proposed so far, also for promoted catalysts, come from model structures which are very far from real catalysts, where the MoS_2 particles are located on nanostructured metal oxide support (often not inert towards sulfiding and reduction treatments) and

are characterized by a multiplicity of structural and valence states. In particular: i) the morphology of the MoS_2 particles is far from the triangular or hexagonal model shape considered in some deeply studied model systems;[13] ii) the particles can be either in form of single slabs or variably stacked; iii) defect sites (edges, corners, sulfur vacancies, stacking faults and others) can be abundantly present and iv) defects induced by the interaction with the support can also contribute to the overall defectivity. In relation to the problem of the importance of the interaction with the support, it is worth to recall that the role of support as "chemical ligand" of the active MoS_2 dispersed phase has been specifically discussed by P.Raybaud.[8] On this basis, a further detailed investigation of the catalysts morphology of the heterogeneity of active sites structure and interaction with the support is desirable.

Herein, the preparation and characterization of MoS_2 HDS catalyst supported on three different metal oxides (SiO_2, γ-Al_2O_3 and MgO) are described. Following our procedure (usually involving CS_2 as sulfiding agent), the supported MoS_2 phases were obtained *in situ* in the experimental cells, where the spectroscopic characterization measurements were performed. In order to have catalysts characterized by similar surface concentration of the active phase, MoS_2 loadings, roughly proportional to the surface area of the supports, were chosen. The structure of the supported MoS_2 phase was characterized by means of several complementary techniques: X-Ray Powder Diffraction (XRPD), X-ray absorption (XAS), Raman and UV-Vis-NIR spectroscopies, which gave information on the structural, vibrational and electronic properties of MoS_2, whereas Transmission Electron Microscopy (TEM) was adopted to determine the morphology of the supported particles. Furthermore, a detailed FTIR analysis of CO adsorbed at low temperature on the *in-situ* prepared samples is reported. To the best of our knowledge, few authors have reported studies of hydrotreating catalysts by means of FTIR of adsorbed CO.[23-25] The most recent contribution on sulfided molybdenum/alumina catalyst comes from the work of Travert *et* al.[26], in which an IR adsorption band in the 2100-2110 cm^{-1} range on samples treated in a H_2S/H_2 atmosphere was attributed to CO adsorbed on the catalytically active sites located at the edges of MoS_2 slabs. The preparation of the catalyst was similar to that adopted in this study, the main difference being represented by the sulfiding step (H_2S, was used instead of CS_2) and by the reducing conditions,(H_2/H_2S was used instead of pure H_2). In some experiments, we used H_2S as sulfiding agent in order to compare our results with those obtained by other researchers and to ascertain the possible role of carbonaceous residues deriving from the sulfidation with CS_2 indetermining the surface structures of MoS_2.

Most of the eexperiments have been performed on catalysts obtained following a sequence of processes mimicking the activation, deactivation and rejuvenation steps of an HDS catalyst. In order to close the gap between the model and the real catalysts, the reactivity of supported MoS_2 particles towards hydrocarbons (which are main components of the industrial reaction mixture) has been also investigated. By comparing the IR spectra of adsorbed CO at the various treatment stages, we were able to follow clearly the changes in the coordination and valence state of Mo sites induced by the different treatments. The presence of several types of reduced Mo^{x+}($X< 4$) species upon prolonged hydrogen treatment at 673 K have been substantiated by parallel UV-Vis experiments. The results obtained for MoS_2 supported on the three different metal oxide supports (SiO_2, γ-Al_2O_3 and MgO) are compared in detail to get information on the role of the support, in determining the surface properties of the active phase. To this end, the careful comparison of the IR spectra of

adsorbed CO on the three systems and the associated morphological details obtained by TEM represent a relevant part of the discussion.

2 Material and Methods

2.1. Samples preparation

We have prepared MoS_2 catalysts supported on SiO_2, γ-Al_2O_3 and MgO, that are three high surface area metal oxides having well known properties. The samples have been synthesized by wet impregnation of SiO_2 (Aerosil: 200 m^2/g), γ-Al_2O_3 (Degussa-Alon C: 100 m^2/g) and $Mg(OH)_2$ (home made: 80 m^2/g) with an aqueous solution of $(NH_4)_6Mo_7O_{24}\cdot 4H_2O$ (Merck, Art. 1182). All the impregnated samples have been subjected to the following preparation steps.

Step 1: drying at 373 K overnight followed by calcination at 723 K for 12 hours and outgassing at 673 K for 1 hour under controlled atmosphere. Then, in order to compensate for possible oxygen lost during thermal activation, 40 mbar of oxygen were dosed at 673 K. Finally, oxygen in excess was outgassed at the same temperature. Under these conditions we have been able to transform the catalyst precursors to MoO_3 supported phase. For MgO support, during the calcination at 723 K, $Mg(OH)_2$ is fully transformed into MgO.

Step 2: sulfiding procedure, where the catalyst was subjected to a treatment in CS_2 atmosphere at 673 K overnight, followed by outgassing at the same temperature for 2 hours under dynamic vacuum, to remove the remaining CS_2.. We wish to underline that, although H_2S and thiophene are the most used sulfur containing molecules used in this step,[15, 27] CS_2 can be used as sulfiding agent as well. The simplicity of the molecular structure, its weak interaction with the surface of the support and the negligible acidic character are in favor of the choice made in this investigation. To be sure that the adoption of CS_2 as sulfiding agent was not substantially altering the final results, in a few cases H_2S was used as sulfiding agent and the results compared with those obtained following the standard procedure.

Step 3: reduction in H_2 atmosphere (two doses of H_2: P_{H2} = 100 mbar at 673 K; total reduction time: 2hrs). After each reduction step the gas phase is removed at 673 K under dynamic vacuum.

Step 4: re-sulfidation in CS_2 atmosphere for 2 hrs (P_{CS2} = 20 mbar at 673 K). Before probing the surface with CO, the gas phase is removed under dynamic vacuum at 673 for 20 min.

It must be underlined that, after the above mentioned steps the systems are outgassed under high vacuum at 673 K. This can have some consequences on the sulfided systems (step 3). In fact, as mentioned in refs. [7, 10] MoS_2 tends to loose sulfur under high vacuum conditions with the consequent alteration on the surface stoichiometry.

Three samples have been analyzed, differing in the Mo loading and in the metal-oxidic support:

(a) MoS_2/SiO_2 (7% wt MoS_2)
(b) MoS_2/γ-Al_2O_3 (4.5% wt MoS_2)
(c) MoS_2/MgO (3% wt MoS_2)

To obtain a comparable surface concentration of the active phase, the adopted MoS_2 loadings were roughly proportional to the surface area of the supports.

2.2. Samples characterization

The morphology of the sulfided samples has been investigated by means of a JEOL 3010-UHR HRTEM microscope operating at 300 kV, equipped with a 2k x 2k pixels Gatan US1000 CCD camera. The samples were deposited on a copper grid covered with a lacey carbon film.

X-Ray Powder Diffraction patterns have been collected with a PW3050/60 X'Pert PRO MPD diffractometer from PANalytical working in Bragg-Brentano geometry, using as source the high power ceramic tube PW3373/10 LFF with Cu anode and equipped with Ni filter to attenuate K_β. Scattered photons have been collected by a RTMS (Real Time Multiple Strip) X'celerator detector: data were collected in the $5 \leq 2\theta \leq 70°$ angular range, with 0.02° 2θ steps.

X-ray absorption (XAS) experiments at the S K-edge (2472 eV) and Mo L_3-edge (2520 eV) were performed simultaneously at the Swiss Synchrotron Radiation Facility (SLS, Zurich, CH) on LUCIA beamline.[28] A Si(111) monochromator was adopted and harmonic rejection was made by using Ni coated mirrors. Due to the particular configuration of the beamline, it was possible to collect in parallel both fluorescence yield (FY) and total electron yield (TEY), allowing us to choose *a posteriori* the spectrum with best signal to noise ratio between the two yields. I_0 was measured via TEY on a 300 nm Ni film sputtered on mylar, I_{1FY} was measured using a Si drift diode detector cooled at -20°C by Peltier effect, and I_{1TEY} was measured with a pico-amperometer. The whole experiment was performed in high vacuum to prevent sample contamination: a special vacuum pipe and a manipulator were used to transfer the samples (activated *ex-situ*) from the glove-box to the measurement chamber. Mo K-edge (20 keV) XAS spectra have been measured at the European Synchrotron Radiation Facility (ESRF, Grenoble, F) on BM26A beamline.[29] All the spectra were collected in transmission mode and the set-up, from source to detector, was as follow: I_0 measured on first ionization chamber (1 bar 40%Ar, 60% He), sample, I_1 measured on a second chamber (2 bar 100% Ar), reference, I_2 measured on a third chamber (0.5 bar 100% Ar). This set-up allows a direct energy/angle calibration for each spectrum avoiding any problem related to little energy shifts due to small thermal instability of the monochromator crystals.[30] The samples have been measured inside a home-made quartz cell, equipped with kapton windows, that allows thermal treatments to be performed in controlled atmosphere.

Raman spectra have been recorded at room temperature (RT) both in air and under controlled atmosphere (using a home made quartz cell) equipped with windows in optical quartz, by using a Renishaw InVia Raman Microscope spectrometer and an Ar^+ laser emitting at 514 nm. A 20X "long working distance" magnification lens has been adopted.

Diffuse reflectance (DR) UV-Vis-NIR spectra of the samples after the sulfidation procedures have been performed on a Cary 5000 Varian spectrophotometer equipped with a diffuse reflectance sphere. To obtain reasonable Kubelka-Munk values the samples were diluted in $BaSO_4$. Before (after step 3) and after reduction in hydrogen (step 4) spectra were recorded on the powdered sample under vacuum in a home made quartz cell equipped with windows in optical quartz.

For FTIR experiments, thin self-supported pellets were used. The spectra were collected on a Bruker IFS 28 Fourier transform spectrophotometer, equipped with cryogenic MCT detector at 2 cm^{-1} resolution. To investigate the state of the surface, the CO probe was dosed on the samples by means of a gas manifold permanently connected to the a home made IR cell allowing to perform thermal treatment under vacuum and gas dosage. The spectra have been collected on samples in

contact with CO pressures in the 0-40 mbar interval. The temperature of the pellet could be gradually varied from 77 to 300 K.

3 Results and discussion

3.1. MoS_2/SiO_2 (7% wt MoS_2)

3.1.1. XRPD, Raman and HRTEM results

XRPD measurements have been performed to demonstrate the effective synthesis of the molybdenum sulfide phase on silica, upon sulfidation of the supported Mo oxide for prolonged time. Upon calcination at 723 K (Step 1) the supported eptamolybdate phase is entirely transformed into MoO_3 (pattern a in Fig. 1). Further treatments in CS_2 atmosphere (P=30 mBar) at 673 K for increasing time (1, 6 and 12h, respectively) transform the supported MoO_3 into MoO_2 (pattern b and c in Fig. 1) and finally into MoS_2 (pattern c and d in Fig. 1).

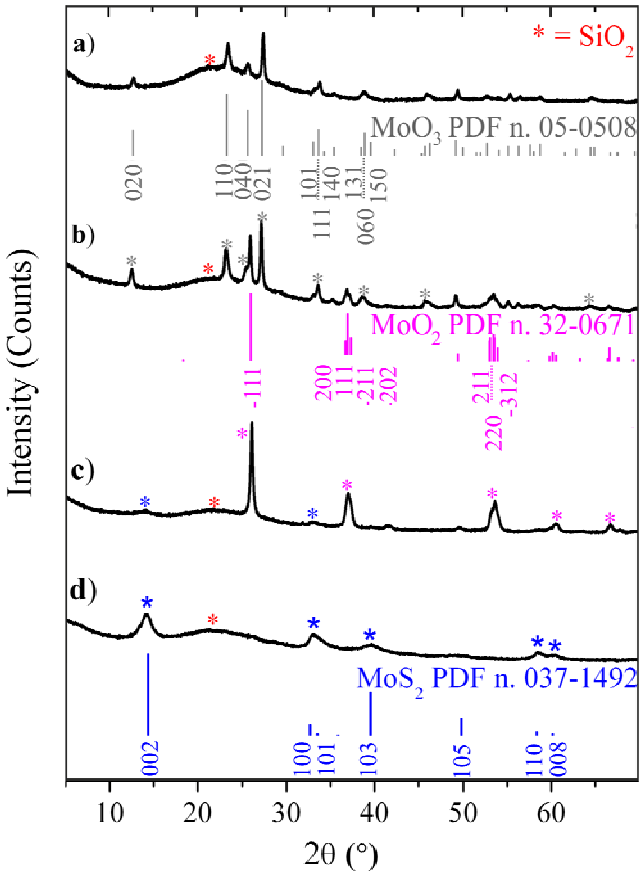

Figure 1. XRPD patterns of the heptamolybdate/SiO_2 after calcinations at 723 K (pattern a) and after the consequent treatment in CS_2 (~ 20 mbar) at 673K for 1h b), 6h c) and 12h d), as compared to the XRD line positions of standard MoO_3 (PDF code number: 005-0508), MoO_2 (PDF code number: 032-0671) and MoS_2 (PDF code number: 37-1492), respectively. Phases are marked by asterisks (red: SiO_2, gray: MoO_3, magenta: MoO_2 and blue: MoS_2).

More in detail, the peaks at 2θ ≈12.8°, 23.4°, 25.7° and 27.4° of the pattern a in Fig. 1 (calcined heptamolybdate phase), are associated to (020), (110), (040) and (021) plane reflections of the MoO_3 phase.The pattern b in Fig. 1 (sulfidation for 1h) shows, in addition to MoO_3 features also

minor reflections at 2θ ≈ 26°, 37° and 53°, associated to plane reflections of the MoO_2 phase. These features become the dominating XRD signals of pattern c in Fig. 1 (sulfidation for 6h). In this pattern, broad XRD signals at 2θ ≈ 14° and 33°of the hexagonal MoS_2, are appearing. Finally, in the pattern shown in Fig.1d, only the peaks of the MoS2 phase are observed. The presence of these peaks (characteristic of MoS_2) and the concomitant disappearance of the MoO_2 peaks, indicate that the sulfidation process is completed after heating the sample for 12 hrs in CS_2 at 673 K.

The XRPD technique used for the control of the sulfidation process, was also adopted to get information on the structure of supported MoS_2. In fact, as the XRD peak broadening depends on the coherent scattering domains, it is possible to determine the crystallite dimensions of the MoS_2 slabs in the c-axis direction by applying the Sherrer's equation ($D_{002} = 0.76 \cdot \lambda / \beta_{002} \cdot \cos\theta$, where λ is the wavelength of the X-Rays, β is the angular full-width-at-half-height FWHM and θ is the diffraction angle),[31] to the (002) XRD diffraction line (see inset of Fig. 2a).

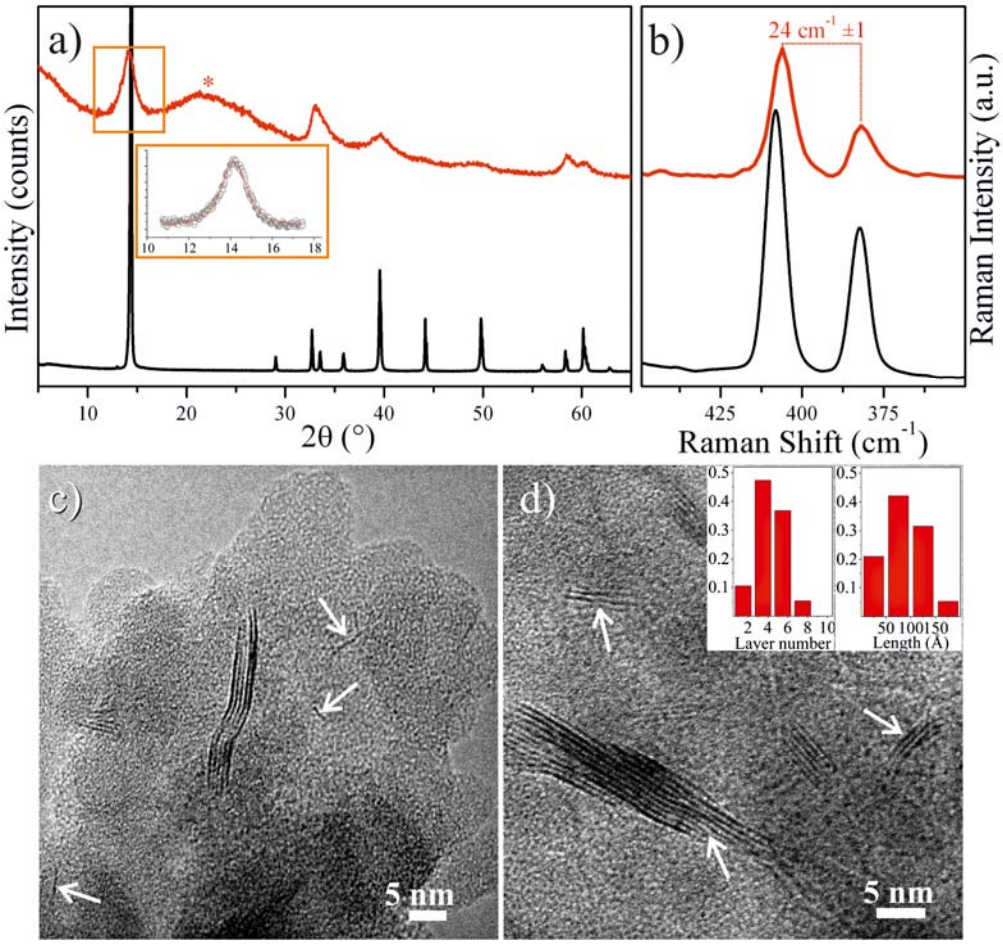

Figure 2. XRPD patterns part a) and Raman spectra part b) of MoS_2/SiO_2 sample after sufidation at 673 K (red line) compared to the reference bulk MoS_2 (black line). Part c) and d) show representative HRTEM images of MoS_2/SiO_2 The arrows indicate the single slab and stacking defects. Inset of a) show a zoom of the (002) XRD diffraction peak of the hexagonal MoS_2 in the 2θ≈ 10-18° range.Insets in part d) show the stacking (layer number) and slab length distributions of MoS_2 layers.

A mean value of about 4 nm was obtained by considering an interlayer distance of 6.17 Å, which indicates a staking number of ≈ 6 layers. As the presence of single MoS_2 layers and the defectivity

(such as imperfect stacking and bending of layers) affects the scattering profile and the (002) XRD diffraction peak as well,[5, 18, 31-35] the evaluation of the average number of slabs following this method is quite approximate and overestimated, as already observed for well dispersed MoS_2 catalysts.[5]The presence of heterogeneous MoS_2 particles characterized by an average staking value of about 6 layers and the high heterogeneity emerging from the analysis of the $2\theta \approx 30°\div50°$ range will be substantially confirmed by the Raman and TEM analyses (see below).

The vibrational properties of the supported MoS_2 phase have been investigated by Raman spectroscopy. The spectrum of the MoS_2 reference sample is reported in Fig. 2b (black curve). According with group theory, four first-order Raman transitions are predicted: E^2_{2g} (at 32 cm^{-1}), E_{1g} (at 287 cm^{-1}), E^1_{2g} (at 383 cm^{-1}), and A_{1g} (at 409 cm^{-1}).[36] E^2_{2g} is too low in energy to be detected by our instrument, E_{1g} is low in intensity (due to the extinction of this mode when *c-axis* is parallel to the scattering path), while E^1_{2g} (vibrations in the basal plane) and A_{1g} (vibrations along the *c* axis, i.e. the stacking direction) have stronger intensities. It has been recently shown[37] that the E^1_{2g} and A_{1g} absorption bands can be used as very informative indicators of the particle staking. In fact, the A_{1g} mode shifts upward from 403 to 408 cm^{-1} on passing from n=1 layer to $n \rightarrow \infty$ (bulk) ($\Delta\nu$= +5 cm^{-1}), while the E^1_{2g} undergoes a smaller downward shift from 384 to 382 cm^{-1}($\Delta\nu$=-2 cm^{-1}). On this basis the frequency difference between these two characteristic Raman bands is considered as indicator of the thickness of the particles. In Fig. 2b the Raman spectrum of MoS_2/SiO_2 sample in the 450-350 cm^{-1} range (red curve) is compared to that of MoS_2 from Fluka (black curve) considered as prototype of perfect bulk counterpart. The frequencies of the characteristic MoS_2 bands in the spectrum of the reference sample closely correspond to those (narrower) reported in the literature for single crystals and consequently their use as reference is justified. The Raman spectrum of the MoS_2/SiO_2 sample shows clearly two absorption bands, which correspond to the characteristic E_{2g} and A_{1g} modes of bulk MoS_2. Following ref. [37], a frequency difference between the two bands of 24 ± 1 cm^{-1} is indicative of particles constituted in average by 6 ± 2 layers. This average stacking degree of the MoS_2 particles is in pretty good agreement with the XRD results discussed above and will be confirmed later by transmission electron microscopy.
From Fig. 2b it is also evident that the E_{2g} and A_{1g} absorption bands in the spectrum of supported particles are broader than the corresponding bands in the spectrum of bulk MoS_2. This might be due to several factors, among which i) a broad distribution of the staking degree (thickness); ii) variable size and shape of the platelets (either single or clustered) and iii) presence of vacancies and other defects influencing the size and planarity of the ordered domains inside the single platelets. A clear cut between these factors cannot be performed.
In conclusion, the Raman spectrum is an useful indicator of the staking and of structural disorder of supported MoS_2 particles. This simple spectroscopic method looks very general and hence will be used also to investigate the dispersion of MoS_2 on Al_2O_3 and MgO.
HRTEM images of the MoS_2/SiO_2 sample (Fig. 2c,d) show that the majority of the SiO_2 surface is covered by structures with high contrast (deep grey zones), which indicate the presence of MoS_2 particles with elongated shape predominantly exposing the basal plane parallel to the electron beam (either single or staked). . The MoS_2 particles with stacking degree ranging from about 8 slabs to single slab are observed., The distribution displayed in the inset shows that most of the particles are characterized by staking values comprised in the 4-6 range. This result is in good agreement with those obtained from XRD and Raman.

Many particles, irrespective of the stacking degree, show clear bending (arrows in Fig. 2c,d), a fact which might be ascribed mainly to the interaction of MoS_2 with the support, although vacancies and dislocations could be invoked as well. Interaction with the support and presence of vacancies are not mutually exclusive. The staking of slabs particles is far from parallel perfection: this also confirm that many types of defects are also present on extended faces, which interfere with the perfect alignment of the slabs. Finally, as for the size of the lamellae is concerned, the inset of Fig. 2d shows that it is mainly comprised in the 5-10 nm range, the lamellae with maximum size (about 10 nm) being observed in the particles with highest staking degree.

3.1.2 EXAFS and XANES results

The supported sulfide phase was analyzed also by means of XAS spectroscopy at S K-edge and Mo L_3 and K-edges, while a wide number of work deals with determination of the MoS_2 local structure by EXAFS analysis, in contrast the electronic configuration and both, metal and ligand atom valence, as obtained by means of XANES analysis on both Mo and S edges are less discussed. Fig. 3a,c shows the XANES spectra of bulk MoS_2 (black curve) and of MoS_2/SiO_2 sample (red curve) at the three different edges, whereas Fig.3d displays the corresponding Mo K-edge EXAFS edge. It is important to evidence that S K- and Mo L_3-edges spectra were collected in fluorescence yield (FY) and thus are more sensitive to surface or near-surface structures and electron configurations, whereas Mo K-edge spectra were measured in transmission mode that is mainly informative on bulk properties.

Starting from the soft X-ray spectra, the S K-edge spectra (Fig. 3a) reflect the dipole allowed transition $1s \rightarrow 3p$ of a core electron of S atoms.. The XANES spectrum of MoS_2 bulk (black curve, Fig. 3a) shows a well defined component at 2470 eV, with an evident shoulder at 2473 eV and first oscillation at 2481 eV. The position of the $1s \rightarrow 3p$ peak is characteristic of a 2- formal valence state. The spectrum of the supported MoS_2/SiO_2 (red curve, Fig. 3a) is very similar to that of bulk MoS_2, but it is characterized by a decrease of the white-line intensity, whereas the shoulder remains unchanged and the first oscillation slightly changes. This behavior can be explained in terms of a preferential orientation of the MoS_2 platelets, enhanced by the polarized nature of X-Ray synchrotron radiation, as already discussed in the work of Guay et al.[38]. In fact, anisotropy in bonding direction for S atoms produces differences in orbital contribution to absorption when slabs are disposed with the stacking axis parallel or perpendicular to the X-Ray beam. Moreover, empty p_x and p_y sulfur orbitals are slightly lower in energy then p_x one, explaining why the white line absorption shows a shoulder at higher energy.[39] Therefore, a change in the orientation of the slabs involves a variation in the white-line intensity, which decreases when beam hit slabs perpendicular to their stacking.[38] Since the sample holder was maintained fixed during the whole experiment, differences in white line structure might be the consequence of a different preferential orientation for pure and supported MoS_2. In particular, it is known that MoS_2 slabs assume preferential orientation when pressed, with stacking axis normal to the holder. This explain why the XANES of bulk MoS_2 resembles those reported in literature for X-Ray beam parallel to c-axis direction,[38] whereas the XANES spectrum of supported catalyst presents contribution coming from differently oriented platelets. This phenomenon is easily explained by considering that platelets in supported MoS_2 follows the morphology of the support in which they are dispersed. This finding fit with TEM results where both dark contrast zone, from flat slabs, and lamellae, from perpendicularly disposed slabs, are present. Unfortunately, this polarization effect does not allow to distinguish the changes induced in the XANES spectrum by the nanometric scale domains.

A few differences between bulk MoS_2 and silica supported catalyst are also present in the Mo L_3-edge spectra, that reflect mainly the $2p \rightarrow 4d$ transition of Mo core electrons (Fig. 3b). In this case, due to the symmetry of Mo site, no polarization effect occurs. Bulk MoS_2 (black curve, Fig. 3b) exhibits an intense and sharp white line without crystal field induced splitting, typical of a Mo species in a trigonal prismatic environment,[40, 41] and a well defined feature centered at 2530 eV. It is worth noticing that the edge is 2.0 eV downward shifted with respect to that of MoO_3 (not reported),[42] as expected by going from a Mo(VI) to a Mo(IV) absorbing species. The spectrum of MoS_2/SiO_2 sample (red curve, Fig. 3b) is very similar to that of bulk MoS_2, but broader and less intense. These differences are ascribed to the nanosized nature of the supported particles.

Coming to hard X-Rays, Mo K-edge XANES spectra are shown in Fig. 3c. The spectrum of bulk MoS_2 sample (black curve, Fig. 3c), has an edge located at 20001 eV, in agreement with an average 4+ oxidation state of Mo cations. At high energy, the spectrum is dominated by a sharp feature at 20015 eV and by a single broad band in the white line region. The spectrum of supported MoS_2 sample (red curve, Fig. 3c) differs from that of the bulk for a partial erosion of the feature at 20015 eV and, at the same time, for an increase of the intensity in the tail of the edge just before the white line (20025 eV). Since the spectrum of molybdenum oxides (MoO_3 and MoO_2)[43] references sample are characterized by a similar behavior, one could interpret the spectrum of MoS_2/SiO_2 as due to the presence of a small residual amount of Mo oxide .[44] However the XRPD and Raman results discussed above and the similitude of the XANES spectrum of our supported MoS_2 XANES sample with that shown by Leliveld et al. [44] for cobalt-molybdenum oxide/γ-Al_2O_3 system let us interpret this result in terms of a weak interaction between MoS_2 and the support.

For Mo K-edge data, the EXAFS part of the spectrum was also collected and the |FT| of the k^3-weighted $\chi(k)$ function of bulk MoS_2 and of silica supported catalyst are reported in Fig. 3d. The |FT| of the EXAFS signal for bulk MoS_2 (black curve, Fig. 3d) presents an intense first shell signal, due to six degenerate Mo-S single scattering (SS) paths at 2 Å and a more intense second shell peak around 3 Å due to six Mo-Mo SS contributions. A less intense and more distant single path contribution and a strong signal at 6.3 Å, due to collinear multiple-scattering Mo-Mo paths enhanced by the focusing effect, are also present, reflecting a high crystalline order(a small difference in the relative Mo-Mo distances it is enough to kill these contributions).

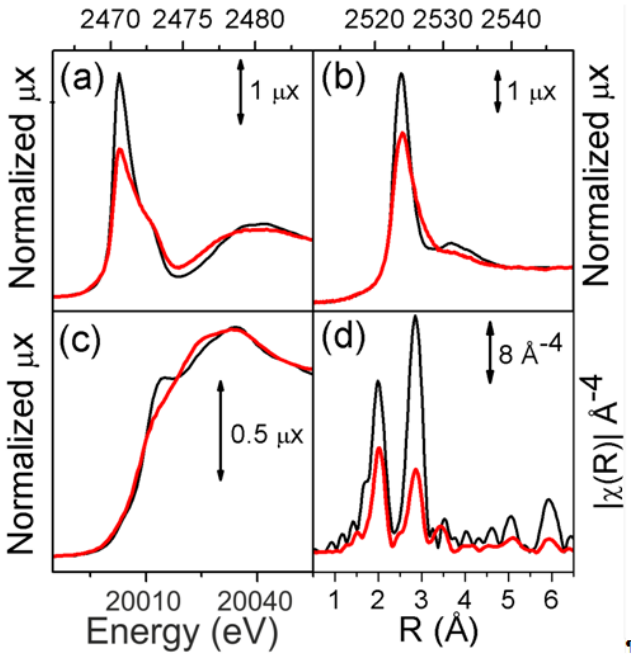

Figure 3. XAS spectra of MoS_2/SiO_2 sample (red curves) and bulk MoS_2 reference (black curves): (a) S K-edge XANES spectra; (b) Mo L_3 edge XANES spectra; (c) Mo-K-edge XANES spectra; (d) k^3-weighted, phase-uncorrected, |FT| of EXAFS spectra collected at the Mo K-edge.

The |FT| of the EXAFS function for MoS_2/SiO_2 sample (red curve, Fig. 3d) is less intense than that of bulk MoS_2 and shows an inversion in the relative intensities of the first and second shell signals. Moreover, the first shell peak has a lower intensity than in the bulk case, meaning that, in average, the Mo absorbing atoms are surrounded by less S neighbours. This behavior is well documented in the case of nanosized and disordered MoS_2 particles.[45-47] As a matter of fact, the debate on the ability of EXAFS to give unambiguous information on the dimensions of MoS_2 slabs, is still open. Shido et al. [47] demonstrated by simulating the experimental data with various clusters that a structural disorder can the same weakening of shell contributions. Other works explain the low value of local order (around 1-3 nm) as due more likely to the extension of ordered sub-domains inside a single slab, instead of the whole extension of the particle.[18, 45-47] Following this interpretation an order extension of 2-3 nm in our case is inferred. A direct comparison with TEM images, which show lateral distribution reaching 10 nm, strongly suggests the hypothesis that MoS_2 platelets in the catalyst are far from being regular and that defects are abundantly present.

3.1.3 UV-Vis results

The UV-Vis-NIR spectrum of the MoS_2/SiO_2 system after complete sulfidation is reported in Fig. 4a (black curve). In the same figure the spectra obtained on the other systems (MoS_2/Al_2O_3 and MoS_2/MgO) are reported for comparison. In Fig. 4b with the spectrum of a thin layer of MoS_2 deposited on a quartz lamina,[48] collected in transmission mode, is also reported.

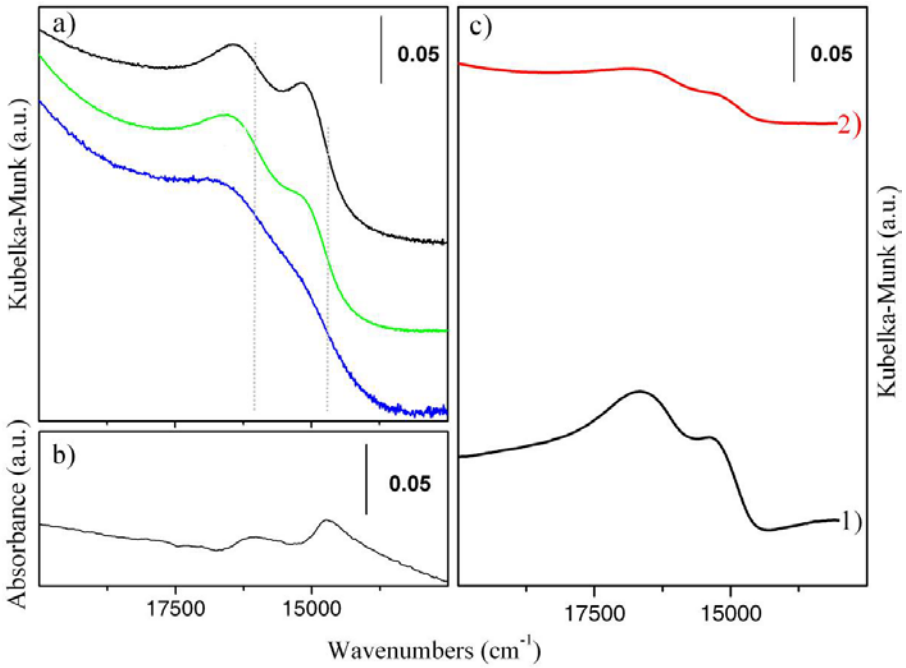

Figure 4. a) UV-Vis-NIR spectra of: MoS_2/SiO_2, MoS_2/Al_2O_3 and MoS_2/MgO samples (black, green and blue curve, respectively) collected in diffuse reflectance mode in air; b) UV-Vis-NIR spectrum of a MoS_2 thin film deposited on an optical quartz window collected in transmission mode in air, ; c) UV-Vis spectra of MoS_2/SiO_2 outgassed (curve 1) and H_2 reduced (curve 2) at 673K, collected in controlled atmosphere in diffuse reflectance mode.

The latter is characterized by two bands at around 16160 and 14730 cm^{-1} which are the two so-called excitonic features associated to the direct transition between d states separated by crystal field effect and split by spin orbit interaction.[49-52] These absorption bands are known as the A_1 and B_1 bands, respectively.[53] The frequency of these bands is influenced by several factors, the major one being represented by the size of the particles, as demonstrated in ref. [54]. In particular the A_1 and B_1 transitions shift to higher frequency upon decreasing the size of the ordered domains. Also the intensity changes with decreasing size of defect-free domains and is expected to decline or vanish in favor of discrete molecular-like transitions when the MoS_2 particle size become very small. On the basis of the literature results[54] and from the observed upward shift on passing from the film to the MoS_2/SiO_2 system we can conclude that the size of the MoS_2 particles on the supported system is definitely lower than that of the reference material. However it is difficult to obtain form the UV-Vis spectra a quantitative information concerning the particle size and the staking value.

The half width of the A_1-B_1 doublet in the spectrum of supported MoS_2 is much higher than that found in the spectrum of the reference film obtained from Fluka sample (which is assumed to be characterized by n= ∞ staking). This is due to the heterogeneity of the particles in the supported MoS_2 and to the contribution of surface states. In fact both phenomena are increasing the width of the excitonic transitions. Another point which merits a specific mention is the significant alteration of the intensity ratio of the A_1-B_1 doublet with respect to reference film. We think that also this effect is associated with the small particle size of supported MoS_2.

The UV-Vis-NIR spectrum of MoS_2/SiO_2 sample outgassed at 673K and collected in controlled atmosphere (vacuum) is illustrated in Fig. 4c. This spectrum is similar to that obtained in air (Fig.

4a), the main relevant difference being represented by an alteration of the intensity ratio of the A_1-B_1 doublet. This effect is plausibly associated with the modification of the interaction with the support associated with the different atmosphere surrounding the particles.
The effect of reduction in hydrogen at 673 K on the UV-Vis-NIR spectrum of MoS_2/SiO_2 (Fig. 4c) is important and can be summarized as follows: a) the absorbance of the sample uniformly increases in the whole visible range; b) the A_1-B_1 doublet can be still observed on the top of the above mentioned continuous absorption, although with reduced intensity. Both effects can be explained by assuming the formation of a MoS_{2-x} phase as a consequence of the reductive removal of stoichiometric sulfur and formation of sulfur vacancies on the corner and edges of the particles (although other defects on basal planes could contribute). In fact as sulfur vacancies are necessarily associated to a multiplicity of reduced states of Mo and hence to the appearance of new d-states in the band gap of MoS_2.[54] (similar to those of isoelectronic Cr^{2+} and Cr^{3+} ions[55]). The formation of a continuum of states is well understood. These states, considered as surface defects and shallow traps[56, 57] are typical of nanosized semiconductors and explain the observed optical features.[58] Notice that the presence of sulfur vacancies is also reducing the extension of the ordered domains necessary for the formation of the excitonic features. This justifies the observed intensity decrease of the A_1-B_1 doublet. In conclusion the UV-Vis-NIR spectra collected under controlled atmosphere give direct proof of the reductive elimination of sulfur and formation of surface vacancies. These sulfur vacancies, being associated with coordinatively unsaturated Mo^{x+}($x<4$) sites, will be probed by CO molecule (*vide infra*).

3.1.4 FTIR spectroscopy of adsorbed CO

As it is widely accepted, information about the properties of coordinatively unsaturated (*cus*) surface sites properties can be obtained from the IR spectra of adsorbed probe molecules (such as H_2, CO and N_2). [55, 59-61] For the scope of this investigation, CO molecule was chosen because of its ability to probe the coordinatively unsaturated (*cus*) M^{x+} species (M= transition metal). In fact, the CO interaction with coordinatively unsaturated metal sites having incomplete d-shell leads to formation of $M(CO)_n$ (n=1-3) complexes, characterized by strong IR bands in carbonyl stretching region (1700-2200 cm^{-1}). The frequency of these bands depends upon the balance between σ donation and π back donation between the metal center and the CO ligand. In very general terms, there is broad consensus that the ν(CO) of carbonyls characterized by prevailing σ donation is higher than that of carbonyls where π back donation is relevant. Another point to be stressed is that the intensity of the ν(CO) bands goes in the opposite direction.[62, 63] In conclusion, the interaction of CO with positively charged centers leads to carbonyls characterized by reduced π back donation (weak bands), while the opposite occurs for CO in interaction with electron rich centers (strong bands). This is the reason why CO is an excellent probe of the coordination and valence state of surface metal centers. A relevant contribution concerning the interaction of CO with Mo^{x+} centers is that of E. Guglielminotti and E.Giamello,[64] where the ν(CO) frequency of carbonyls formed on Mo(V), Mo(IV), Mo(III), Mo(II) and Mo(0) species is considered and determined experimentally. The data reported in ref. [64] are in agreement with the literature on homogeneous molybdenum complexes (see for instance refs. [65-69]).
Fig. 5a reports the evolution of the FTIR spectra (in the CO stretching region) of CO adsorbed at 77 K on sulfided MoS_2/SiO_2 system (i.e. after the sulfidation step), upon decreasing coverage (θ). At

high coverage values (bold gray curve) the spectrum is dominated by an intense and out of scale band at 2157 cm^{-1}, which has been already attributed to CO adsorbed on silanols present on the surface of the SiO_2 support, and by a strong band at 2138 cm^{-1}, due to physically adsorbed (liquid-like) CO. These IR absorption bands are easily reversible upon outgassing at 77 K and both can be ascribed to CO adsorbed on the support. We cannot exclude a contribution to the 2138 cm^{-1} band of CO adsorbed on the planar faces of MoS_2. In fact, due to the absence of coordinatively unsaturated centers, these faces can only interact with CO via physical (dispersive) forces. In the 2130-2000 cm^{-1} range, other significant (although weak) IR absorption bands are present. In particular, at $\theta(CO)_{max}$, a band at 2068 cm^{-1} (with a shoulder at 2073 cm^{-1}) is well evident, accompanied by two minor features at 2115 and 2028 cm^{-1}. Although the species responsible of all these absorptions are more resistant to outgassing than CO species interacting with the support and with the planar faces as well, the corresponding IR bands decrease in intensity upon decreasing CO pressure. These bands must be attributed to a small fraction of carbonylic species formed on coordinatively unsaturated Mo centers.

Fig. 5b,c report the evolution of the FTIR spectra of CO adsorbed at 77 K on MoS_2/SiO_2 sample after H_2 reduction and after re-sulfidation at 673 K, respectively. Also in this case, the spectra are dominated by the characteristic bands due to the adsorption of CO on the SiO_2 support (2157-2138 cm^{-1}). The constant intensity of the 2157 cm^{-1} band upon different activation and sulfidation conditions indicates that no appreciable transformation of silanols into -SH groups and that no appreciable sulfidation of the silica surface are occurring. However, it is evident that the bands in the 2130-2000 cm^{-1} range are significantly affected by the activation treatment. In particular, the IR absorption band at 2115 cm^{-1} becomes the most prominent one upon reduction (Fig. 5b), whereas it almost disappears upon re-sulfidation (Fig. 5c). All these bands, which are red-shifted with respect to the free CO molecule (ν_{CO} = 2143 cm^{-1}), can be attributed to the interaction of CO with coordinatively unsaturated Mo^{x+} cations. Following refs. [64-66, 68, 69] the involved valence states should be lower than IV. The shift with respect to the 2143 cm^{-1} value of the ν(CO) gas can be ascribed to the effect of π back-donation of the *d* electrons of Mo towards the CO anti-bonding orbitals, as observed in classical linear metal carbonyls. These coordinatively unsaturated molybdenum ions are associated with sulfur vacancies preferentially formed on samples reduced in hydrogen. It is however difficult to give a more detailed assignment of all the single bands, since, beside the σ-π balance in linear species, other additional factors can affect the IR frequency of adsorbed CO oscillators. In particular, we have to consider that CO adsorbed at a sulfur vacancy position can interact in a bridged form with more than one Mo ion, a fact that can have profound effect on the stretching frequency (as well known when the frequency of linear and bridged carbonyls are compared). On this basis the only safe conclusion that can be derived from the analyses of the IR spectrum is that the presence of more than one absorption band reflects a complex surface situation, most probably associated with different oxidation states and different coordinative unsaturation of Mo centers located at the sulfur vacancies positions on the edges and corners of the disordered particles (possibly not excluding also some defect present on the basal faces).

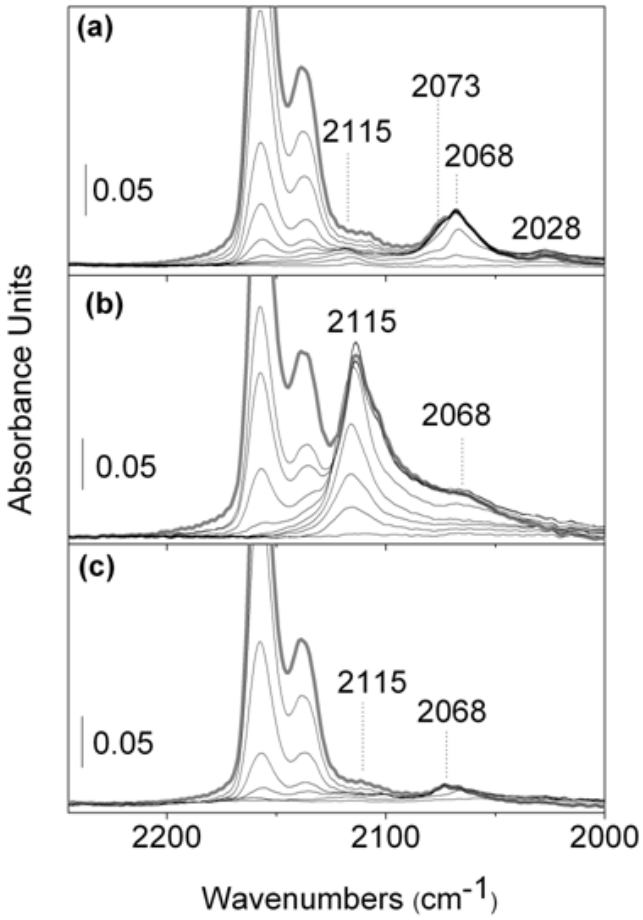

Figure 5. FTIR spectra of CO adsorbed at 77 K on MoS_2/SiO_2 sample outgassed at 673 K (**a**), H_2 reduced at 673 K (**b**) and treated in CS_2 atmosphere at 673 K (**c**). The evolution of the spectra upon decreasing coverages (θ) is reported (θ_{max} = 20 mbar, bold grey curve).

The hypothesis that coordinatively unsaturated Mo^{x+}(x<4) centers could be responsible for the CO absorption bands in the 2115-2000 cm^{-1} range has been already discussed in literature. In particular, it has been reported that CO adsorption on MoS_2 catalysts (treated in H_2/H_2S atmosphere) supported on Al_2O_3 gives rise to a main absorption band at 2110 cm^{-1} and a broad band at 2070 cm^{-1}, with a tail extending to 2000 cm^{-1}. The main band has been ascribed to CO adsorbed on the catalytically active sites located at the edges of MoS_2 slabs.[23, 26, 70, 71] The activity of these sites is thought to be associated with sulfur ions vacancies, *i.e.* coordinative unsaturation. For example, Elst *et* al. attributed two IR absorption bands at 2106 and 2065 cm^{-1} to active edge and corners sites of MoS_2 slabs, respectively.[7] Our data are in good agreement with this assignment. It is worthy noticing that the observed frequencies can be justified only if CO interacts with Mo^{x+} species in reduced states (x< 4). The hypothesis that reduced Mo ions are involved in the formation of carbonyls seems in conflict with the presence of low intensity of the IR bands in the 2068-2028 cm^{-1} range on the sulfided sample not treated in hydrogen at 673 K (Fig. 5a). About this point let us however recall that the sulfided samples were always outgassed at 673 K under high vacuum before CO dosage. As it well known that under high vacuum MoS_2 looses sulfur (a fact which have prevented so far the study of MoS_2 single crystals under ultra high vacuum conditions), the obtained results are not surprising. This hypothesis is confirmed by the results of experiments (not reported for brevity), where CO is dosed on samples outgassed at lower temperature (no carbonylic bands are present). It

is quite conceivable that under high vacuum conditions at 673 K sulfur vacancies can be formed on the most exposed sites, where sulfur anions show the lowest coordination. We do not exclude that the weak band at 2028 cm^{-1} could be due to a small amount of $Mo^0(CO)_n$ species formed by reduction of Mo ions in very exposed corner positions. Due to the well known increment of the extinction coefficient of IR absorption bands due to carbonyls characterized by increasing back donation, the species absorbing in the 2068-2028 cm^{-1} range could be associated with very low concentrated species.

In conclusion, on the basis of the experimental results and of the literature data concerning the IR spectroscopy of molybdenum carbonyls, it can be inferred that: i) the IR absorption bands observed in the spectra shown in Fig. 5 are associated with coordinatively unsaturated Mo species in a valence state lower than 4+ and that these sites become exposed to the interaction of with CO, because of the formation of sulfur vacancies; ii) the IR absorption band at 2115 cm^{-1}, which grows mostly after reduction in H_2 at 673 K, is due to carbonyls formed on species Mo^{x+} ($x < 4$) located on edge sites (because, considering the inertness of the basal planes, they are the most abundant reducible structures), being the formation of these reduced species in pure H_2 at 673 K in agreement with TPR results (data not shown); iii) the Mo species associated with the 2068 cm^{-1} absorptions, which are formed by simple activation in vacuo at 673 K, are due to reduced Mo^{x+} ($x < 4$) species associated with surface sulfur vacancies located on very exposed sites (for instance corner sites); iv) we do not exclude that the weak band at 2028 cm^{-1} could be due to a small amount of $Mo^0(CO)_n$ species formed by reduction of Mo ions in very exposed corner positions; v) whatever is the assignment of each IR absorption band, the complexity of the IR spectrum demonstrates that on highly dispersed MoS_2 particles characterized by a different size, irregular shape, variable staking degree and presence of a variety of defects, several types of sulfur vacancies (and hence of coordinatively unsaturated, Mo^{x+}($x<4$) centers can exist, which once probed with CO, give a variety of IR signals. We also note that, under the adopted treatment conditions at 673 K (prior to CO contact) no clear IR absorption band at about 2600 cm^{-1}, indicative of the formation of SH species on MoS_2 phase was observed (spectra not shown).

To verify whether the sulfidation with CS_2 is equivalent to the most commonly performed process, that make use of H_2S, we have studied the adsorption of CO on samples sulfided with H_2S under equivalent conditions. As the obtained spectra (reported in the supplementary information), are nearly equivalent to those illustrated in Fig. 5a-c, we can conclude that the spectra obtained on samples sulfided using CS_2 are fully representative of the catalyst system. Another consequence of this result is that carbonaceous impurities possibly deriving from the use of CS_2 instead of H_2S do not sensibly influence the surface chemistry of MoS_2.

As final consideration let us underline that the picture emerging from the IR spectroscopy results is fully confirming the results obtained by UV-Vis spectroscopy.

3.2. MoS_2/γ-Al_2O_3 (4.5 % wt MoS_2)

It is known that by changing the oxide support of the industrial HDS catalysts a significant change in their activity is induced. Many scientific works have highlighted these experimental results and key questions about the influence of the support on industrial HDS catalysis have been formulated. Furthermore, it is known that a control of acidic-basic character of the supports can promote a high and stable dispersion of MoS_2 and should also inhibit coke formation. In particular, γ-Al_2O_3 has

received great attention as catalytic support because of its outstanding structural and morphological properties and its relatively low cost. As for MoS_2/SiO_2, the XRD, HRTEM and Raman results will give information on the dispersion of the supported MoS_2 phase. FTIR of adsorbed CO, will be discussed in detail because it has been demonstrated to be the most sensitive technique for the detection of surface coordinatively unsaturated Mo species.

3.2.1 XRD, HRTEM, Raman and UV-Vis results

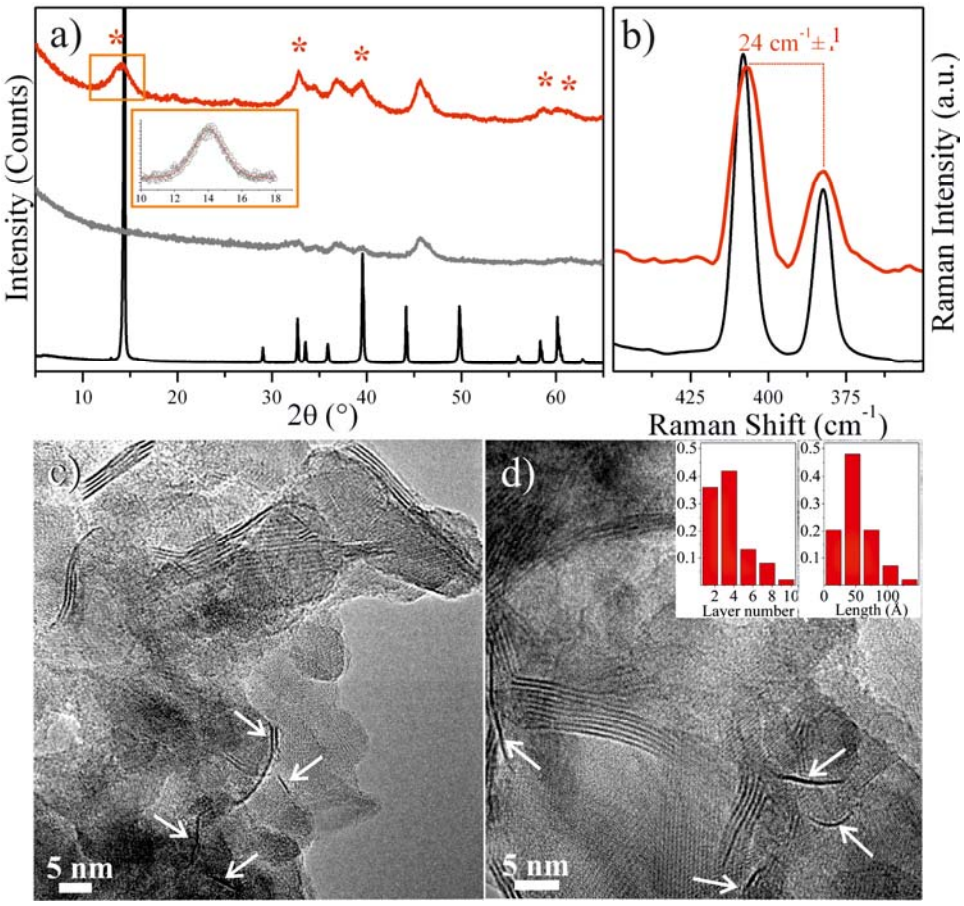

Figure 6. XRPD patterns a) and Raman spectra b) of: MoS_2/γ-Al_2O_3 (x2, red line), γ-Al_2O_3 (gray line, only in the XRD part), and reference bulk MoS_2 (black line); HRTEM images c) and d) of MoS_2/γ-Al_2O_3 sample after sulfination at 673 K. In the inset, the (002) XRD diffraction peak of the MoS_2/γ-Al_2O_3 (x4) in the 2θ~10-18° range. The arrows in c) and d) indicate single and double slabs, defective stacking and bended layers. In the insets of d) distributions of the layer numbers and lengths of MoS_2 layers, are reported.

In Fig. 6a, the X-ray diffraction patterns of γ-Al_2O_3 (gray line) and of MoS_2/γ-Al_2O_3 (red line) samples are reported, together with that of the standard MoS_2 (Fluka) (black line). The XRPD pattern of MoS_2/γ-Al_2O_3 reveals the presence of three broad peaks at 37.6°, 45.7° and 66.7°, which can be assigned to γ-Al_2O_3 support, while the five peaks labeled with the asterisks are ascribed to MoS_2 phase (PDF n. 037-1492). As discussed for MoS_2 /SiO_2, the application of the Sherrer's equation to the (002) XRD peak allows to determine the average crystallite dimensions of the MoS_2 slabs in the c-axis direction and hence the staking degree. A mean value of about 5 layers is

obtained, thus indicating that the dispersion of MoS_2 on Al_2O_3 is better than on SiO_2, considering also the fact that few nanometers single stacked particles escape from XRD detection.
Likewise, Raman spectrum of MoS_2/γ-Al_2O_3 is reported in Fig. 6b (red curve) and shows only the two vibrational E_{2g} and A_{1g} modes of bulk MoS_2 associated with sulfide phase. The frequency difference between the two peaks is 24 ± 1 cm^{-1} system is indicative that, in average, the particles are constituted by 6 ± 2 layers, as for MoS_2/SiO_2. Moreover, the E_{2g} and A_{1g} bands in the spectrum of supported particles are broader than the corresponding bands of bulk MoS_2, and even broader than those observed on MoS_2/SiO_2 system. This is likely due to a larger distribution of the staking degree (including a major fraction of single platelets) and is indicative of a larger heterogeneity.
Representative TEM images of MoS_2/γ-Al_2O_3 sample are reported in Fig. 6c,d. Multi-layered MoS_2 platelets, with a distribution of the stacking degree up to 5÷7 layers, and numerous single dark lines, corresponding to single-layered MoS_2 platelets are observed. The monolayer MoS_2 platelets are curved and follow to the curvature and shape of the γ-Al_2O_3 support (arrows in Fig. 6c,d). This behavior is more pronounced with respect to that observed for MoS_2/SiO_2, so suggesting that in MoS_2/γ-Al_2O_3 a larger interaction of the MoS_2 platelets with the substrate is present, a fact which favors dispersion. In the inset, the staking distribution as derived from HRTEM shows that most of the particles are characterized by staking comprised in the 1-4 layer range, a datum which is in agreement with XRD and Raman results. In the same figure an inset concerning the size distribution is also presented which shows that the size of most platelets is 5 nm.
Compared to the MoS_2/SiO_2 the MoS_2 platelets on γ-Al_2O_3 look definitely smaller, hence justifying the broader character of the Raman bands and the Vis spectrum of the MoS_2/γ-Al_2O_3 (Fig. 4a) showing a broadening and a shift to higher frequency of the excitonic peaks .

3.2.2 The FTIR of adsorbed CO

Fig. 7a reports the evolution of the FTIR spectra of CO adsorbed at 77 K on MoS_2/γ-Al_2O_3 sample, upon decreasing coverage (θ) in the 2300-1950 cm^{-1} range.

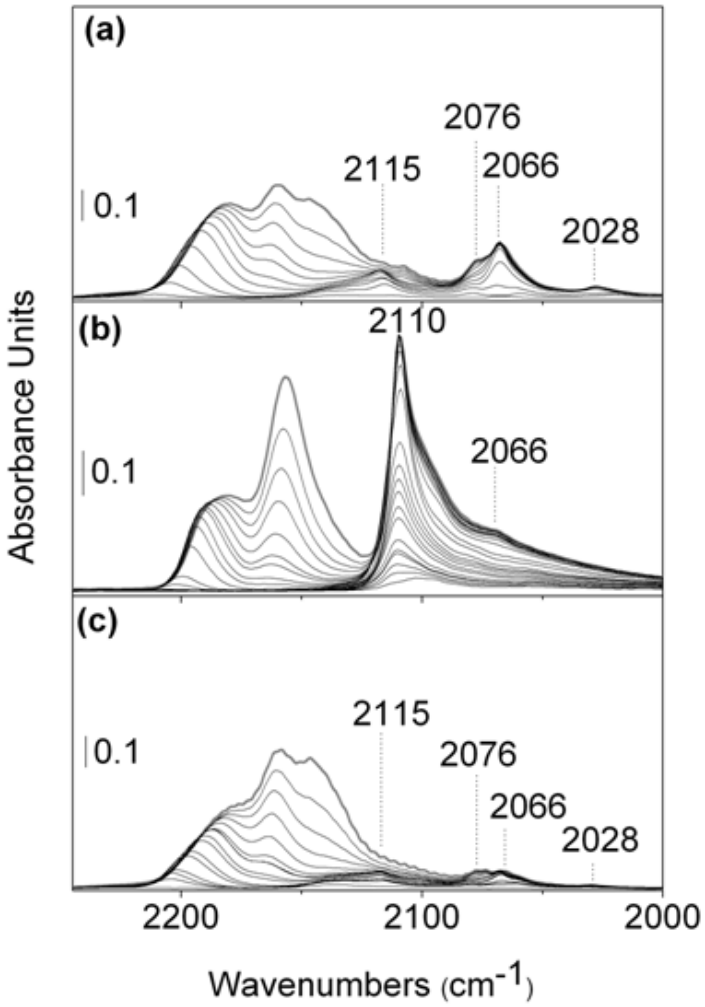

Figure 7. FTIR spectra of CO adsorbed at 77 K on MoS_2/γ-Al_2O_3 sample outgassed at 673 K (**a)**, H_2 reduced at 673 K (**b**) and treated in CS_2 atmosphere at 673 K (**c**). The evolution of the spectra upon decreasing coverages (θ) is reported (θ_{max} = 20 mbar, bold grey curve).

The MoS_2/γ-Al_2O_3 catalyst was subjected to the same *in-situ* pre-treatment procedures carried out for MoS_2/SiO_2 systems (see Section 3.1.2). FTIR spectra of CO adsorbed on MoS_2/γ-Al_2O_3 outgassed at 673 K are dominated by three main IR absorption bands centered at 2184, 2157 and 2140 cm^{-1} at $\theta = \theta_{max}$, which decreases in intensity and shift in frequency by decreasing the CO coverage. These IR absorption bands are entirely due to CO in interaction with the γ-Al_2O_3 support, although CO physically adsorbed on the basal planes of the MoS_2 platelets can contribute as well. It must be underlined that the spectrum in the 2184-2140 cm^{-1} range is not identical to that observed when CO is dosed on pure γ-Al_2O_3. On the reason of this difference we shall return in the following. As already observed for MoS_2/SiO_2 system, additional significant IR absorption bands are present in the 2130-2000 cm^{-1} range, which are attributed to the interaction of CO with Mo^{x+} (x< 4) cations on the surface of MoS_2 crystallites. The frequency of each band is practically the same observed in the spectrum of MoS_2/SiO_2, indicating that we are in presence of the same species. The major difference is represented by the bands intensity, which is definitely higher on MoS_2/γ-Al_2O_3. This confirms the increased dispersion of MoS_2 on γ-Al_2O_3 support, already shown by TEM and other techniques. Notice that the IR absorption bands associated with CO on Mo^{x+} (x < 4) centers undergo an evolution upon H_2 reduction (Fig. 7b) and re-sulfidation in CS_2 (Fig. 7c) at

673 K in the same way as observed for MoS_2/SiO_2. Also in this case the formation and removal of sulfur vacancies upon sulfiding and reducing conditions is then demonstrated.
As a final comment, unlike MoS_2/SiO_2, the IR absorption bands attributed to CO adsorbed on the γ-Al_2O_3 support are altered by the treatment conditions. In particular, only the spectrum recorded after treatment in H_2 at 673 K is identical to that of CO adsorbed on pure γ-Al_2O_3. Although it is outside the scope of this work, we mention that preliminary FTIR experiments performed on pure γ-Al_2O_3 treated with CS_2 show that a partial sulfidation of the γ-Al_2O_3 surface occurs and that the effect on the IR spectrum in the 2184-2140 cm^{-1} range is similar to that observed in Fig. 7. This process is mainly due to $O^{=}/S^{=}$ substitution on a fraction of the most reactive sites. The treatment of MoS_2/SiO_2 in H_2 at 673 K removes the sulfur species from Al_2O_3 surface and consequently the spectrum of absorbed CO becomes identical to that obtained by dosing CO on pure γ-Al_2O_3. Notice also that under the adopted treatment conditions at 673 K no IR absorption bands clearly due to SH groups were observed, on both the support and on MoS_2 phase.

3.3. MoS_2/MgO (3 % wt MoS_2)

MgO, having basic character, differs from other common metal-oxidic supports, which are usually acidic or neutral. Its basicity might be favourable for the MoS_2 dispersion, because of increased interaction between acidic MoO_3 anhydrides and MgO surfaces. A reduced tendency to form coke is also expected for basic support materials. Hydrodesulfurization activity of MgO-supported MoS_2 catalysts has been found to be higher than that of γ-Al_2O_3-supported MoS_2 systems. The higher activities were attributed to the increased dispersion of MoS_2 on MgO surface.

3.3.1 XRD, HRTEM, Raman and UV-vis results

Fig. 8a shows the X-ray diffraction patterns of MgO pretreated with CS_2 (blank experiment, S-doped MgO: gray line) and of MoS_2/MgO (red line) samples, as well as the pattern of the standard MoS_2 (black line).

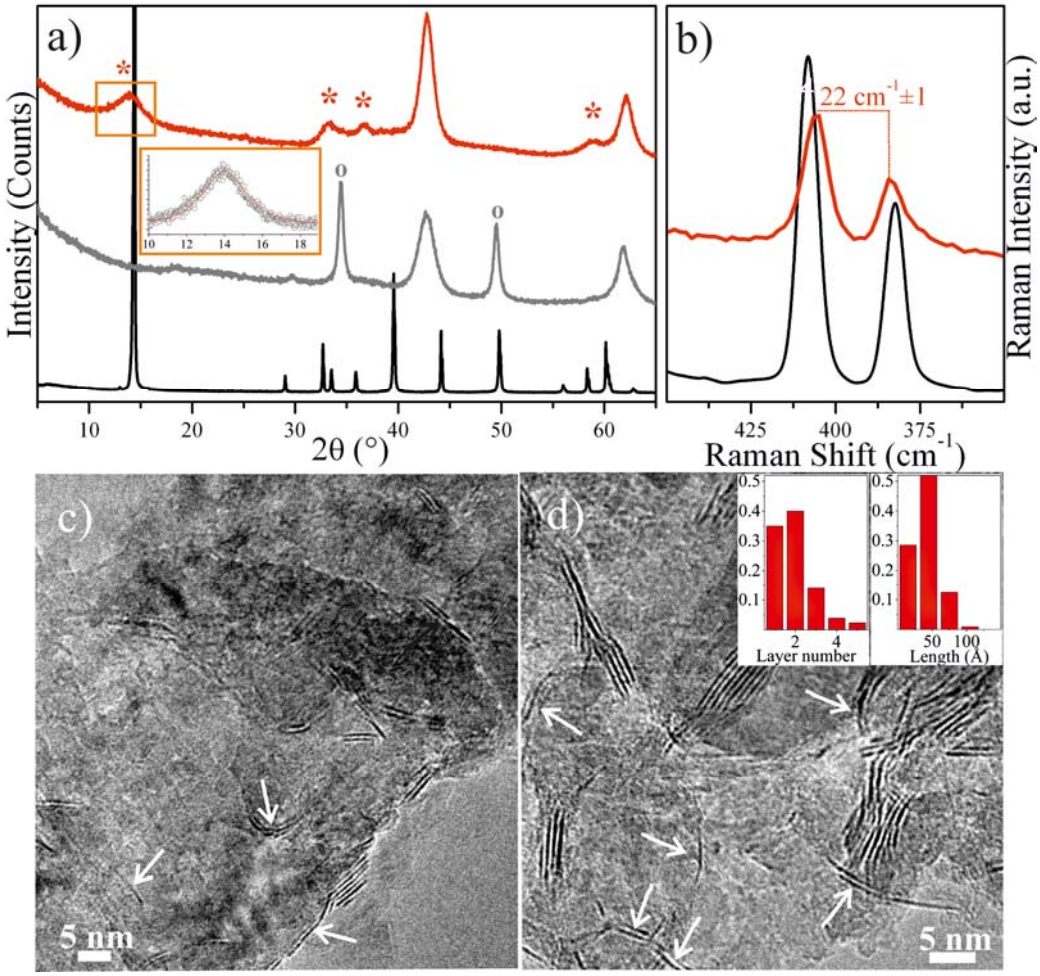

Figure 8. XRPD patterns a) and Raman spectra b) of: S-doped MgO (gray line, only in the XRD part), MoS_2/MgO (red line) and reference bulk MoS_2 (black line); HRTEM images of MoS_2/MgO sample, as outgassed at 673 K c) and d). In the inset, the (002) XRD diffraction peak of the MoS_2/MgO (x4) in the 2θ~10-18° range. The arrows in c) and d) indicate single slabs and defective stackings of MoS_2 layer. In the insets of d) distributions of the layer numbers and lengths of MoS_2 layers, are reported.

The XRPD pattern of MoS_2/MgO system reveals, together with the characteristic peaks of MgO, also four reflections (labeled with the asterisks) due to MoS_2 (PDF n. 037-1492). The pattern of S-doped MgO, shows two broad peaks (2θ ≅ 42.6° and 61.8°), which are ascribed to the (200) and (220) crystalline planes of MgO phase, and three narrow peaks (2θ ≅ 29.7°, 34.4° and 49.4°), labeled with the circles, that can be assigned to (111), (200) and (220) reflection planes of MgS phase. This result clearly demonstrates that pure MgO support can react with sulfur containing molecules not only altering the surface $O^{=}/S^{=}$ ratio, but also forming crystalline MgS. However, the latter phase is not present on the MoS_2/MgO system. The reason of the inhibitory effect of MoS_2 on the formation of bulk MgS is not known. As made for MoS_2/SiO_2 and MoS_2/γ-Al_2O_3 systems, the Sherrer's equation has been applied to the (002) XRD peak to determine the average crystallite dimensions of the MoS_2 slabs in the c-axis direction and, hence, the staking degree. A mean value of about 2 layers is obtained, thus indicating that on MgO the MoS_2 dispersion is higher that that observed on both γ-Al_2O_3 and SiO_2.

The Raman spectrum of MoS_2/MgO fully confirms this result (Fig. 8b). In fact, the frequency difference between the E_{2g} and A_{1g} vibrational modes of bulk MoS_2[8] is now 22 ± 1 cm^{-1}, which indicates that the contributing particles are constituted by 3± 1 layers in average. This mean stacking degree of the MoS_2 particles is in pretty good agreement with that obtained from XRD results. The broad character of the bands indicates that the system is highly heterogeneous.
The morphological properties of the MoS_2/MgO system are shown in Fig. 8c,d. HRTEM images reveal that many single slabs are present, together with platelets having a distribution of the stacking degree between 3 and 8 layers. The lateral dimension of the platelets is in the 5-10 nm range. Single and double layered MoS_2 platelets are often curved, because they conform to the curvature of the support particles (arrows in Fig. 8c,d). This fact suggests that MoS_2-support interaction is enhanced even with respect to MoS_2/γ-Al_2O_3. In most cases the curvature of the platelets is so evident that the presence of defects induced by interaction with MgO surface must be invoked. These defects interrupt the planarity and regularity of the platelets and hence increase the system heterogeneity. We speculate that the enhanced interaction of MoS_2 platelets with the MgO surface and the tendency of the support to undergo $O^{=}/S^{=}$ exchange are intimately connected and that the role of the support to act as "chemical ligand" of the MoS_2 platelets is influenced by the presence of $S^{=}$ ions on the matrix.[62]
As evidenced in the staking distribution derived from HRTEM (Inset of Fig. 8d), most of the particles are characterized by staking comprised in the 1-2 layer range, in agreement with XRD results. The basal size distribution (right inset in Fig. 8d) is centered around 5 nm, although the distribution does not consider the effect of the curvature. The small size of MoS_2 platelets can justify both, the broad character of the Raman bands and the UV-vis spectrum of the MoS_2/MgO system illustrated in Fig. 4a. In fact, the broadening of the excitonic peaks and the shift to higher frequency can be fully explained on the basis of a decrement of the platelets size, on the presence of curvature and on a lowered staking degree.

3.3.2 FTIR spectra of adsorbed CO

The evolution of the FTIR spectra of CO adsorbed at 77 K on MoS_2/MgO sample, upon decreasing coverage (θ) is reported in Fig. 9. The strong IR absorption bands observed in the 2180-2150 cm^{-1} range are associated with the stretching modes of CO species physically adsorbed on the supporting matrix.[62] Similarly to what observed for the MoS_2/γ-Al_2O_3 system, this part of the spectra changes as a function of treatment conditions. A detailed discussion about this point is again outside the scope of the paper and we only mention that this effect is due to a change in the surface structure and composition of MgO upon sulfidation. Only the spectrum of CO adsorbed on the sample reduced in H_2 at 673 K is identical to that of CO adsorbed on pure MgO matrix. These results demonstrate that sulfidation and reduction in H_2 have no effect not only on MoS_2 but also on the MgO support. As already discussed for MoS_2/SiO_2 and MoS_2/γ-Al_2O_3 systems, the IR absorption bands in the 2170-2030 cm^{-1} range are attributed to CO interacting with Mo^{x+} ($x < 4$) species of MoS_2 platelets. These bands show an evolution induced by the treatments substantially similar to what observed for MoS_2/SiO_2 and MoS_2/γ-Al_2O_3 samples.

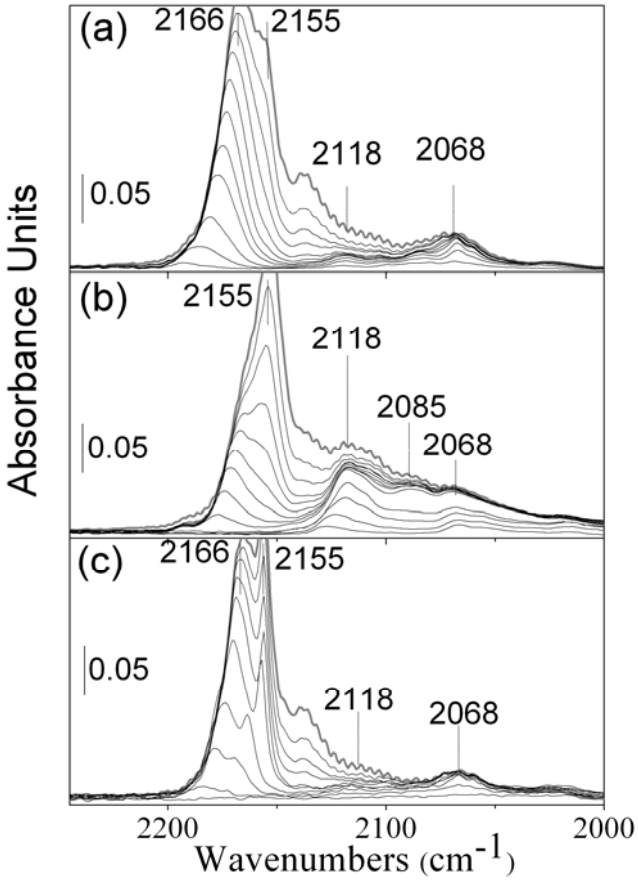

Figure 9. FTIR spectra of CO adsorbed at 77 K on MoS_2/MgO sample outgassed at 673 K (a), H_2 reduced at 673 K (b) and treated in CS_2 atmosphere at 673 K (c). The evolution of the spectra upon decreasing coverages (θ) is reported (θ_{max} = 20 mbar, bold grey curve).

From the spectra evolution upon H_2 reduction (Fig. 9b), it can be highlighted that: i) the intensity of the band at 2118 cm^{-1} increases; ii) a new broad band grows at 2085 cm^{-1}, iii) the band at 2068 cm^{-1} is substantially unaffected and iv) the IR bands in the 2120-2000 cm^{-1} range are broader than those observed on the other systems. As for the sample re-sulfided in CS_2 atmosphere at 673 K (Fig. 9c), we highlight that the IR absorption band at 2118 cm^{-1} is preferentially affected and that this result is again similar to those obtained for MoS_2/SiO_2 and MoS_2/γ-Al_2O_3 systems. All these facts confirm that molybdenum sites can be reduced, with reversible production and saturation of sulfur vacancies.

4 Conclusions

Supported MoS_2 model systems were obtained from the supported oxide precursor phase on three different metal oxides (SiO_2, γ-Al_2O_3 and MgO), structural, optical and vibrational investigation techiques confirmed the validity of our synthesis to obtain well dispersed MoS_2 nanoparticles. The adopted procedure, which is based on the use of CS_2 instead of the classical H_2S/H_2 mixture in autoclave, is very simple and leads to complete sulfidation of the supported MoO_3 phase, suggesting that CS_2 has the dual function of sulfidation and reducing agent. XRD measurements performed at increasing sulfidation stages have been used to set up the best procedure for the in situ synthesis of

MoS_2/silica. This procedure was successively adopted also to obtain the MoS_2/γ-Al_2O_3 and MoS_2/MgO systems. XANES analysis confirms the expected S and Mo valences for the MoS_2 structure, whereas S K-edge measurements revealed that MoS_2 platelets adopt a preferential orientation to follow the support structure. From both, EXAFS signal and TEM images we verified that the supported MoS_2 platelets are highly defective.

By examining the XRD, Raman and UV-Vis the staking and the size of the supported MoS_2 platelets have been determined. The application of the Sherrer's equation to the (002) XRD peak of MoS_2 allowed to determine the average crystallite dimensions of the MoS_2 slabs in the c-axis direction, hence the staking degree on all samples is decreasing from ~6 and 4 (MoS_2/SiO_2 and MoS_2/γ-Al_2O_3) to ~ 2 (MoS_2 /MgO). Also the Raman spectra of supported MoS_2 gave valuable information about the structure of supported MoS_2. In fact, the frequency difference between the two E_{2g} and A_{1g} vibrational modes of supported MoS_2 resulted to be a sensitive probe of the staking degree, while the broad character of the corresponding bands was a qualitative indicator of particle heterogeneity. Although the general trend is the same, staking figures obtained from Raman data are slightly higher than those obtained by the other methods, because the Raman signal from particles characterized by highest staking is more intense. The application of UV-vis spectroscopy has demonstrated a great utility in the (qualitative) determination of two parameters: particle size and presence of sulfur vacancies induced by hydrogen reduction. In particular, it has been ascertained beyond any doubt that reduction in hydrogen at 673K causes the formation of a variety of coordinatively unsaturated Mo^{x+} sites characterized by $x < 4$ and that the presence of these reduced states profoundly alters the optical properties of the systems. It is worth underlining that the afore mentioned physical methods are of simple application and therefore can be utilized to monitor the dispersion of the active phase in industrial catalysts in a fast semi-quantitative way.

HRTEM pictures confirmed the coexistence and the dispersion degree of single and stacked MoS_2 slabs having basal dimension never exceeding 10 nm. However, great differences among the three supports can be highlighted: in fact, a decrease of the average staking degree from 4-6 in MoS_2/SiO_2 to 2-4 in MoS_2/γ-Al_2O_3 and to 1-2 in MoS_2/MgO is inferred. The effect on the basal size of platelets is less important as it decreases from about 10 nm (MoS_2/SiO_2) to 5 nm (MoS_2/γ-Al_2O_3, MoS_2/MgO). From these data and from the observation that slabs are intimate curved following the profile of the support particles, it is inferred that the interaction between the MoS_2 and the support increases by moving from SiO_2 to γ-Al_2O_3 to MgO and reflects the increasing dispersion of catalyst particles. In this regard, we mention the fact that sulfidation process has its influence also on the supporting matrix. In fact, MgO incorporates sulfur in the structure, γ-Al_2O_3 show surface reactivity, while SiO_2 does not show reactivity at all. .

Considering that both the HDS activity and the tendency of the three investigated supports to undergo $O^{=}/S^{=}$ exchange follow the order MoS_2/MgO> MoS_2/γ-Al_2O_3 > MoS_2/SiO_2 and that the same order is verified for the particle dispersion, it is hypothesized that all these factors are strongly linked and that the incorporation of $S^{=}$ ions in the surface of the support is influencing the MoS_2/support interaction.

The results obtained from the FTIR spectroscopy of CO adsorbed at 77 K on MoS_2/oxide samples allowed to obtain direct information on the nature of the *cus* sites involved in the HDS reaction, showing that: i) outgassing the completely sulfided particles at 673 K under high vacuum is enough to reduce a small number of Mo sites probably located on corners and other exposed positions. Evidence of the formation of a low amount of Mo^0 species is also found. On the contrary, samples

outgassed only at 373 K do not show any evidence of reduced Mo sites; ii) treatment in hydrogen at 673 K causes the formation of new and abundant low valence Mo^{x+} (x<4) species (the corresponding carbonyls giving an IR absorption band at 2115 cm^{-1}) most likely located on edges. The reduction of Mo ions located on flat surfaces in correspondence of defects is however not excluded. CO is only physically adsorbed on defect free portions of the flat MoS_2 surfaces which are not exposing coordinatively insaturated sites and are very resistant to hydrogen reduction.; iii) thermal treatment in CS_2 at sufficiently high temperature (673 K) is able to restore almost completely the starting sulfide phase, with the consequent disappearance of the Mo sites associated with sulfur vacancies on edge sites. The complexity of the IR spectra of adsorbed CO demonstrates that on highly dispersed catalyst, MoS_2 particles characterized by large size dispersion, irregular shape, variable staking degree, presence of a variety of defects, and several types of sulfur vacancies (and hence of coordinatively unsaturated Mo^{x+}(x<4)) centres coexist, which originate a variety of surface carbonyls and IR absorption bands once probed with CO. Finally, let us underline that the similarity of the results of IR of adsorbed CO on MoS_2 supported on the SiO_2, γ-Al_2O_3 and MgO supports excludes that the carbonyl bands can be due to Mo^{x+} species directly anchored to the supports.

The whole set of data reported herein directly face the problem of the nature of the active sites in MoS_2-based HDS catalysts and bring evidence that the surface concentration of sulfur vacancies associated with low valence Mo^{x+} (x<4) species can be reversibly formed by changing the activation conditions (reduction or sulfidation). These vacancies are mostly located on corner and edge sites. However, considering the highly disordered nature of the samples and the remarkable curvature of the MoS_2 platelets particularly evident on γ-Al_2O_3 and MgO, the presence of sulfur vacancies also on flat surfaces is not excluded. Finally, the participation of the γ-Al_2O_3 and MgO supports in the sulfidation/reduction steps is also demonstrated.

Acknowledgements

We are indebted with the whole staff of the beamlines LUCIA, at the SLS, and BM26 DOUBBLE, at the ESRF, where soft and hard XAFS experiments have been performed; in particular with M. Janousch (LUCIA) and with S. Nikitenko (BM26) for their competent and friendly support.

This work was supported by MIUR (Ministero dell'Istruzione, dell'Università e della Ricerca), INSTM Consorzio and Eni S.p.A.

References

1 H. L. Zhang, K. P.; Sow, C. H.; Gu, H. R.; Su, X. D.; Huang, C. & Chen, Z. K., *Langmuir*, 2004, **20**, 6914-6920.

2 N. B. Barreau, J. C., *Journal of Physics D-Applied Physics*, 2002, **35**, 1197-1204.

3 L. B. Rapoport, Y.; Feldman, Y.; Homyonfer, M.; Cohen, S. R. & Tenne, R., *Nature*, 1997, **387**, 791-793.

4 J. P. Wilcoxon, *Journal of Physical Chemistry B*, 2000, **104**, 7334-7343.

5 M. P. De la Rosa, S. Texier, G. Berhault, A. Camacho, M. J. Yacaman, A. Mehta, S. Fuentes, J. A. Montoya, F. Murrieta and R. R. Chianelli, *Journal of Catalysis*, 2004, **225**, 288-299.

6 M. U. Kouzu, K.; Kuriki, Y. & Ikazaki, F., *Applied Catalysis a-General*, 2004, **276**, 241-249.

7 R. R. Chianelli, M. H. Siadati, M. P. De la Rosa, G. Berhault, J. P. Wilcoxon, R. Bearden and B. L. Abrams, *Catalysis Reviews-Science and Engineering*, 2006, **48**, 1-41.

8 P. Raybaud, *Applied Catalysis a-General*, 2007, **322**, 76-91.

9 L. E. Elst, S.; van Langeveld, A. D. & Moulijn, J. A., *Journal of Catalysis*, 2000, **196**, 95-103.

10 J. F. C. Paul, S. & Payen, E., *Catalysis Today*, 2008, **130**, 139-148.

11 N. Topsoe, *Journal of Catalysis*, 1980, **64**, 235-237.

12 J. D. Grimblot, P.; Gengembre, L. & Bonelle, J.-P., *Bulletin des Sociétés Chimiques Belges*, 1981, **90**, 1311.

13 J. V. B. Lauritsen, M. V.; LÃ¦gsgaard, E.; Jacobsen, K. W.; NÃ¸rskov, J. K.; Clausen, B. S.; TopsÃ¸e, H. & Besenbacher, F., *Journal of Catalysis*, 2004, **221**, 510-522.

14 J. V. N. Lauritsen, M.; NÃ¸rskov, J. K.; Clausen, B. S.; TopsÃ¸e, H.; LÃ¦gsgaard, E. & Besenbacher, F., *Journal of Catalysis*, 2004, **224**, 94-106.

15 H. C. Topsoe, B. S. & Massoth, F. E., *Science and Technology in: Hydrotreating Catalysis*, Springer, Berlin, 1996.

16 N. R. Dinter, M.; Raybaud, P.; Kasztelan, S.; da Silva, P. & Toulhoat, H., *Journal of Catalysis*, 2009, **267**, 67-77.

17 H. C. Topsoe, B. S.; Topsoe, N. Y. . & Pedersen, E., *Industrial and Engineering Chemistry Fundamentals*, 1986, **25**, 25-36.

18 C. Calais, N. Matsubayashi, C. Geantet, Y. Yoshimura, H. Shimada, A. Nishijima, M. Lacroix and M. Breysse, *Journal of Catalysis*, 1998, **174**, 130-141.

19 N. Y. T. Topsoe, H., *Journal of Catalysis*, 1993, **139**, 631-640.

20 P. H. Raybaud, J.; Kresse, G.; Kasztelan, S. & Toulhoat, H., *Journal of Catalysis*, 2000, **189**, 129-146.

21 S. P. Cristol, J. F.; Payen, E.; Bougeard, D.; Clemendot, S. & Hutschka, F., *Journal of Physical Chemistry B*, 2000, **104**, 11220-11229.

22 S. P. Cristol, J. F.; Payen, E.; Bougeard, D.; Clemendot, S. & Hutschka, F., *Journal of Physical Chemistry B*, 2002, **106**, 5659-5667.

23 B. v. L. Mueller, A. D.; Moulijn, J. A. & Knoezinger, H., *The Journal of Physical Chemistry*, 1993, **97**, 9028-9033.

24 J. B. Peri, *The Journal of Physical Chemistry*, 1982, **86**, 1615-1622.

25 M. I. V. Zaki, B. & Knoezinger, H., *The Journal of Physical Chemistry*, 1986, **90**, 3176-3183.

26 A. D. Travert, C.; Mauge, F.; Cristol, S.; Paul, J. F.; Payen, E. & Bougeard, D., *Catalysis Today*, 2001, **70**, 255-269.

27 M. L. Vrinat, *Applied Catalysis*, 1983, **6**, 137-158.

28 A. M. C. Flank, G.; Lagarde, P.; Bac, S.; Janousch, M.; Wetter, R.; Dubuisson, J. M.; Idir, M.; Langlois, F.; Moreno, T. & Vantelon, D., *Nuclear Instruments & Methods in Physics Research Section B-Beam Interactions with Materials and Atoms*, 2006, **246**, 269-274.

29 S. B. Nikitenko, A. M.; van der Eerden, A. M. J.; Jacques, S. D. M.; Leynaud, O.; O'Brien, M. G.; Detollenaere, D.; Kaptein, R.; Weckhuysen, B. M. & Bras, W., *Journal of Synchrotron Radiation*, 2008, **15**, 632-640.

30 C. B. Lamberti, S.; Bonino, F.; Prestipino, C.; Berlier, G.; Capello, L.; D'Acapito, F.; Xamena, Fxli & Zecchina, A., *Physical Chemistry Chemical Physics*, 2003, **5**, 4502-4509.

31 G. Berhault, M. P. De la Rosa, A. Mehta, M. J. Yacaman and R. R. Chianelli, *Applied Catalysis a-General*, 2008, **345**, 80-88.

32 P. Joensen, E. D. Crozier, N. Alberding and R. F. Frindt, *Journal of Physics C-Solid State Physics*, 1987, **20**, 4043-4053.

33 P. Joensen, R. F. Frindt and S. R. Morrison, *Materials Research Bullettin*, 1986, **21**, 457-461.

34 Y. Y. Peng, Z. Y. Meng, C. Zhong, J. Lu, W. C. Yu, Z. P. Yang and Y. T. Qian, *Journal of Solid State Chemistry*, 2001, **159**, 170-173.

35 K. S. Liang, R. R. Chianelli, F. Z. Chien and S. C. Moss, *Journal of Non-Crystalline Solids*, 1986, **79**, 251-273.

36 T. J. V. Wieting, J. L., *Physical Review B*, 1971, **3**, 4286.

37 C. Lee, H. Yan, L. E. Brus, T. F. Heinz, J. Hone and S. Ryu, *Acs Nano*, 2010, **4**, 2695-2700.

38 D. Guay, W. M. R. Divigalpitiya, D. Belanger and X. H. Feng, *Chemistry of Materials*, 1994, **6**, 614-619.

39 L. F. Mattheiss, *Physical Review B*, 1973, **8**, 3719 LP - 3740.

40 R. H. Coehoorn, C. & de Groot, R. A., *Physical Review B*, 1987, **35**, 6203.

41 G. N. C. George, W. E.; Enemark, J. H.; Smith, B. E.; Kipke, C. A.; Roberts, S. A. & Cramer, S. P., *Journal of the American Chemical Society*, 1990, **112**, 2541-2548.

42 T. T. Ressler, O.; Neisius, T.; Find, J.; Mestl, G.; Dieterle, M. & Schlogl, R., *Journal of Catalysis*, 2000, **191**, 75-85.

43 T. W. Ressler, J.; Jentoft, R. E. & Neisius, T., *Journal of Catalysis*, 2002, **210**, 67-83.

44 R. G. v. Leliveld, A. J.; Geus, J. W. & Koningsberger, D. C., *Journal of Catalysis*, 1997, **171**, 115-129.

45 S. P. Bouwens, R.; Debeer, V. H. J. & Koningsberger, D. C., *Journal of Physical Chemistry*, 1990, **94**, 3711-3718.

46 E. J. M. K. Hensen, P. J.; van der Meer, Y.; van der Kraan, A. M.; de Beer, V. H. J.; van Veen, J. A. R. & van Santen, R. A., *Journal of Catalysis*, 2001, **199**, 224-235.

47 T. P. Shido, R., *Journal of Physical Chemistry B*, 1998, **102**, 8426-8435.

48 K. M. Garadkar, A. A. Patil, P. P. Hankare, P. A. Chate, D. J. Sathe and S. D. Delekar, *Journal of Alloys and Compounds*, 2009, **487**, 786-789.

49 J. P. N. Wilcoxon, P. P. & Samara, G. A., *Journal of Applied Physics*, 1997, **81**, 7934-7944.

50 K. K. P. Kam, B. A., *The Journal of Physical Chemistry*, 1982, **86**, 463-467.

51 A. A. K. Akl, H. & Abdel-Hady, K., *Applied Surface Science*, 2006, **252**, 8651-8656.

52 G. L. E. Frey, S.; Homyonfer, M.; Feldman, Y. & Tenne, R., *Physical Review B*, 1998, **57**, 6666-6671.

53 A. Splendiani, L. Sun, Y. B. Zhang, T. S. Li, J. Kim, C. Y. Chim, G. Galli and F. Wang, *Nano Letters*, 2010, **10**, 1271-1275.

54 B. L. Abrams and J. P. Wilcoxon, *Critical Reviews in Solid State and Materials Sciences*, 2005, **30**, 153-182.

55 E. L. Groppo, C.; Bordiga, S.; Spoto, G. & Zecchina, A., *Chemical Reviews*, 2005, **105**, 115-183.

56 L. Brus, *The Journal of Physical Chemistry*, 1986, **90**, 2555-2560.

57 L. Brus, *Journal of Physics and Chemistry of Solids*, 1998, **59**, 459-465.

58 J. C. Ramirez, L. & Busca, G., *Journal of Catalysis*, 1999, **184**, 59-67.

59 A. Zecchina, S. Coluccia and C. Morterra, *Appl. Spectrosc. Rev.*, 1985, **21**, 259-310.

60 A. Zecchina and C. O. Arean, *Chem. Soc. Rev.*, 1996, **25**, 187-&.

61 A. Zecchina, D. Scarano, S. Bordiga, G. Spoto and C. Lamberti, in *Advances in Catalysis, Vol 46*, ACADEMIC PRESS INC, San Diego, 2001, vol. 46, pp. 265-397.

62 A. Zecchina, D. Scarano, S. Bordiga, G. Ricchiardi, G. Spoto and F. Geobaldo, *Catalysis Today*, 1996, **27**, 403-435.

63 C. Lamberti, E. Groppo, A. Zecchina and S. Bordiga, *Chem. Soc. Rev.*, In press.

64 E. Guglielminotti and E. Giamello, *Journal of the Chemical Society, Faraday Transactions 1: Physical Chemistry in Condensed Phases*

J. Chem. Soc., Faraday Trans. 1, 1985, **81**, 2307-2322.

65 W. S. Tsang, D. W. Meek and A. Wojcicki, *Inorganic Chemistry*, 1968, **7**, 1263-1268.

66 M. H. Chisholm, J. A. Connor, J. C. Huffman, E. M. Kober and C. Overton, *Inorganic Chemistry*, 1984, **23**, 2298-2303.

67 C. C. Williams and J. G. Ekerdt, *Journal of Physical Chemistry*, 1993, **97**, 6843-6852.

68 T. Szymanska-Buzar, T. Glowiak and I. Czelusniak, *Inorganic Chemistry Communications*, 2001, **4**, 183-186.

69 X. Z. Sun, S. M. Nikiforov, A. Dedieu and M. W. George, *Organometallics*, 2001, **20**, 1515-1520.

70 B. M. K. Vogelaar, N.; van der Zijden, T. F.; van Langeveld, A. D.; Eijsbouts, S. & Moulijn, J. A., *Journal of Molecular Catalysis a-Chemical*, 2009, **309**, 79-88.

71 Z. L. S. Wu, F. X.; Wu, W. C.; Feng, Z. C.; Liang, C. H.; Wei, Z. B. & Li, C., *Journal of Catalysis*, 2004, **222**, 41-52.

Model oxide supported MoS_2 HDS catalysts: structure and surface properties

Federico Cesano[a],Serena Bertarione[a], Andrea Piovano[a], Giovanni Agostini[a], Mohammed Mastabur Rahman[a], Elena Groppo[a], Francesca Bonino[a], Domenica Scarano[a], Carlo Lamberti[a], Silvia Bordiga[a], Luciano Montanari[b], Lucia Bonoldi[b], Roberto Millini[b] and Adriano Zecchina[a*]

[a]*Department of Inorganic, Physical and Materials Chemistry, NIS Centre of Excellence, and Centre of Reference INSTM, University of Turin, Via P. Giuria 7, I-10125, Torino, Italy*
[b] *Eni S.p.A., Refining & Marketing Division, Research and Technological Development, Research Center, Via Maritano 26, I-20097 San Donato Milanese (MI), Italy*

Supporting information

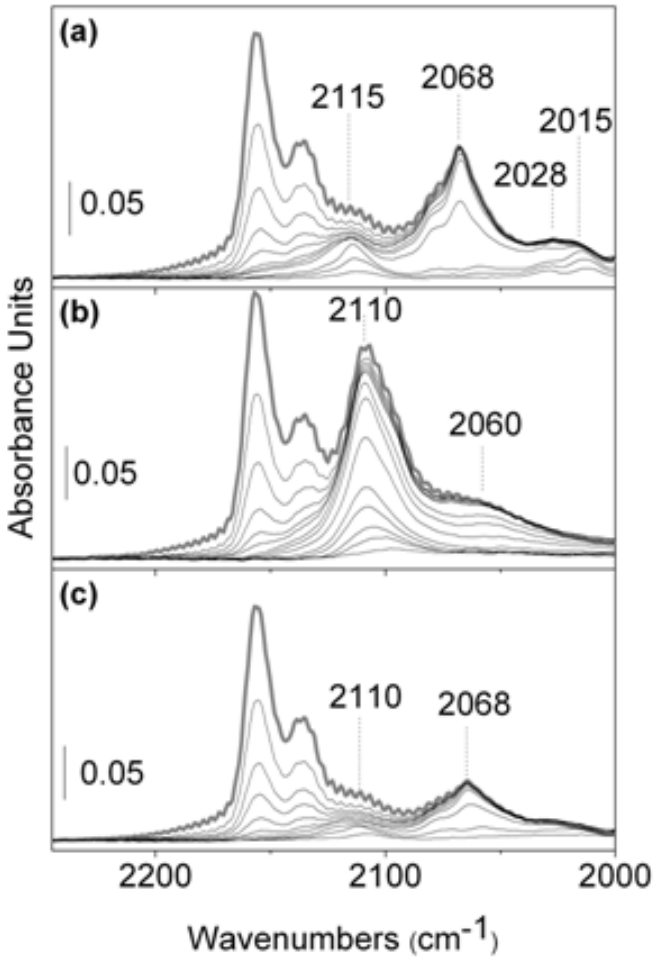

Figure SI 1. FTIR spectra of CO adsorbed at 77 K on MoS_2/SiO_2 sample outgassed at 673 K (a), H_2 reduced at 673 K (b) and treated in H_2S atmosphere at 673 K (c). The evolution of the spectra upon decreasing coverages (θ) is reported (θmax = 20 mbar, bold grey curve).